Comparative Analysis of Indole Derivative Production Among Clinical Isolates of *Fusobacterium nucleatum*

Colin Scano[1], Ankan Choudhury[2], Macarena G. Rojo[3], Ramon Lavado[3], Greg Zaharas[1], Jessalyn Hawkins[1], Leigh Greathouse[1,2]

1. Biology Department, Baylor University

2. Robbins College of Health and Human Sciences, Baylor University

3. Environmental Science, Baylor University

Corresponding Author: Leigh Greathouse

Objectives: To investigate how indole production modulates *Fusobacterium nucleatum* virulence across different disease states.

Methods: Total indole production was measured in 16 *F. nucleatum* isolates (CRC: n=6, Crohn's: n=6, healthy: n=3, oral: n=1) using Kovac's reagent. Disease-associated indole derivatives—indole, indole-3-acetic acid (IAA), indole-3-aldehyde (I3A), indole-3-carboxaldehyde (I3CA), and indole-3-propionic acid (IPA)—were quantified via HPLC. Isolates were treated with exogenous derivatives to assess impacts on biofilm formation and virulence gene expression. A naïve Bayes classifier trained on virulence factor data evaluated niche-specific responses.

Results: CRC isolates produced significantly more total indole than healthy isolates ($p<0.05$). Indole derivatives minimally affected non-CRC isolate growth but reduced CRC isolate carrying capacity. Total indole positively correlated with biofilm formation in CRC isolates ($R^2=0.50$-0.70; $p<0.001$). Crohn's isolates formed most biofilm but were unresponsive to indoles; CRC isolates showed reduced formation. A Naïve Bayes classifier accurately predicted disease association from indole-induced virulence factor expression (AUC=0.90-0.92, Accuracy=0.74-0.75; $p<2e-16$).

Conclusions: CRC-associated isolates show unique metabolic profiles with elevated indole production and respond distinctively to indole exposure, suggesting potential therapeutic targets.

INTRODUCTION

Since the discovery that *F. nucleatum* selectively colonizes colorectal cancer (CRC) tissue (1,2), numerous studies have investigated how this bacterium both directly and indirectly contributes to CRC pathogenesis. Without known DNA-damaging toxins, *F. nucleatum* relies on type V secretion systems with outer membrane proteins that facilitate bacterial interactions (e.g. CmpA, RadD, aid1) (3,4), and host cell binding (e.g. RadD, Fap2, FadA) (5–8). Despite extensive research on host responses to *F. nucleatum* virulence factors, the regulatory mechanisms governing virulence expression differences among clinical isolates and subspecies remain poorly characterized. Given indoles' established role in modulating microbial virulence, investigating how *F. nucleatum* senses, metabolizes, and regulates indole production is essential for understanding and potentially controlling its pathogenic behavior.

Indole is a key bacterial signaling molecule that regulates collective behaviors and modulates epithelial responses to gut pathogens (9). *F. nucleatum*, a producer of indoles via Trp metabolism, has been shown to modulate its biofilm formation—a hallmark of CRC (10,11)—in response to indole exposure (12). More than 85 gram-positive and gram-negative species are known to hydrolyze tryptophan into the parent compound indole via the tryptophanase enzyme (tnaA) (13). Indole derivatives, through activation of aryl hydrocarbon receptor (AhR) and pregnane X receptor (PXR), regulate intestinal function and are increasingly investigated for their potential to modulate chemotherapy efficacy in cancer treatment (14). However, the impact of increased indole concentrations on CRC-associated pathogens remains poorly understood. While elevated indole levels have been shown to enhance biofilm formation in an oral *F. nucleatum* isolate (12), the mechanisms by which indole derivatives influence biofilm development and virulence in CRC-associated *F. nucleatum* strains are still unclear.

F. nucleatum is a central component of oral biofilms, bridging commensals and pathogens (15), and is believed to be the source of colon-derived *F. nucleatum* (16). In the CRC microenvironment, *F. nucleatum* is selectively enriched in biofilm-positive colon tumors (11). These *F. nucleatum*-positive biofilms are associated with reduced E-cadherin expression, increased IL-6/STAT3 signaling, and heightened crypt cell proliferation in adjacent normal colonic mucosa (10). Understanding the mechanisms that regulate *F. nucleatum* biofilm formation is therefore critical to elucidating its role in CRC progression.

This study aimed to characterize indole production profiles of clinical *F. nucleatum* isolates across various disease associations, with particular emphasis on determining whether increased indole derivative concentrations modulate isolate virulence. We conducted targeted HPLC analysis across 16 *F. nucleatum* clinical isolates from healthy individuals or those with disease and evaluated how indole exposure affects biofilm formation and virulence factor expression. Results revealed distinct indole production profiles among isolates, with CRC-associated isolates demonstrating significantly elevated production of indole derivatives. Notably, CRC-associated isolates exhibited heightened sensitivity to indole exposure, resulting in concentration-dependent decreases in biofilm formation. In contrast, the oral lesion strain ATCC 25586, which is

extensively cited in literature, displayed increased biofilm formation in response to indole exposure, indicating environment-specific differential responses to indole among isolates. These findings reveal a novel direction for investigating the regulatory mechanisms underlying *F. nucleatum* virulence, with potential implications for therapeutic interventions targeting indole-mediated pathways.

MATERIALS AND METHODS

Bacterial growth conditions: *F. nucleatum* cultures were prepared by streaking glycerol stocks onto Columbia blood agar plates containing L-cysteine (0.5 g/L), hemin (5 mg/L), vitamin K (10 µg/L), and 5% defibrinated sheep blood. Plates were incubated anaerobically (90% N_2, 5% CO_2, 5% H_2) at 37°C for 48-72 hours. Single colonies were transferred to anaerobically reduced Columbia broth and grown under identical anaerobic conditions at 37°C for 24-48 hours before dilution and use in experiments. Culture purity was regularly confirmed through Gram staining.

Biofilm formation Assay: Biofilm formation by *F. nucleatum* isolates was assessed using previously described methods (12) with the following modifications. Biofilm biomass was quantified through crystal violet (CV) staining in 96-well plates. Planktonic cells were removed from 96-well plates and biofilms were washed once with sterile water, then air-dried for 5 minutes. Biofilms were fixed with methanol at 37°C overnight. Fixed biofilms were stained with 0.1% crystal violet for 1 minute, washed with deionized water until control wells were clear, and air-dried for 5 minutes. Biofilms were destained with 30% acetic acid for 5 minutes. Absorbance was measured at 560 nm using a Sunrise Tecan microplate reader with 10-second shaking before measurement and analyzed with SparkControl software (v2.3).

Time course Biofilm Assay Single colonies were grown anaerobically in Columbia broth to stationary phase (48 hours), then diluted to 0.3 OD_{600}. The diluted culture was used to inoculate six 96-well plates simultaneously, with two wells per plate left uninoculated for contamination monitoring and background correction. Plates were collected at specific timepoints (12, 24, 36, 48, 60, and 72 hours), measured for optical density (OD600) using a Cerillo Stratus plate reader, and subsequently processed using the previously described biofilm formation assay.

Growth curves and indole treatment: To assess the impact of indole derivatives on *F. nucleatum* growth, sixteen isolates were cultured anaerobically in Columbia broth and treated with five compounds: indole, indole propionic acid (IPA), indole-3-acetic acid (IAA), indole-3-aldehyde (I3A), and indole-3-carboxylic acid (I3CA). Stock solutions were prepared in DMSO and diluted to final concentrations of 0.25, 0.5, 1, and 2 mM. DMSO-only controls were used to normalize solvent concentration. Tryptophan (1.25–10 mM) was used to assess bacteria's ability to convert tryptophan into indole affected their growth, and chloramphenicol (12.5–100 µg/mL) as negative controls. Mid-log phase cultures were diluted to a standardized OD_{600} (0.3), and each treatment was plated in triplicate. Growth curves were generated in a Cerillo Stratus reader (96-well format) at 37°C under anaerobic conditions for 72 hours, with OD_{600} measured hourly.

113 *Quantification of total indole production with Kovacs reagent:* *F. nucleatum* isolates were
114 streaked from frozen stocks, and liquid cultures were initiated from single colonies. Starter
115 cultures were grown to stationary phase, then diluted to 0.3 OD_{600}. for inoculation. Media
116 conditions included Columbia broth, Columbia + 5 mM tryptophan, Columbia + 1%
117 glucose, and BHI complete (with 0.5 g/L L-cysteine, 5 mg/L hemin, 10 µg/L vitamin K).
118 Each media type was aliquoted into deep-well 96-well plates (1.2 mL/well) and inoculated
119 with diluted culture. Samples were collected every 12 hours over 72 hours (0–72 h), and
120 100 µL of culture was frozen at –20°C for indole quantification. Indole quantification was
121 performed according to previously established methods (17). Briefly, samples were
122 thawed slowly at 4°C, then centrifuged at 3,000 g for 15 minutes to pellet the bacteria.
123 The supernatant was transferred to a new 96-well plate and mixed with an equal volume
124 of Kovac's reagent. After a 5-minute color development period, the OD560 was measured
125 with shaking for 10 seconds on a plate reader (Sunrise Tecan's Magellan™ universal
126 reader). Indole concentrations were determined using a standard curve generated with
127 synthetic indole at concentrations ranging from 0 to 2000 µM.

128 *Indole Derivative quantification by HPLC:* *F. nucleatum* isolates were streaked from
129 frozen stocks and cultured in liquid medium from single colonies. Starter cultures were
130 grown to stationary phase, then diluted to 0.3 OD_{600} for inoculation. Each isolate was
131 subsequently inoculated into Columbia broth and incubated for 48 hours, after which
132 cultures were centrifuged and supernatants collected. Indole derivatives in the
133 supernatant were analyzed using high-performance liquid chromatography (HPLC) with
134 fluorescence detection, following modified methods from Tuomola et al. (18) and Kema
135 et al. (19). Chromatographic separation was performed on an UltiMate 3000 HPLC
136 system equipped with an RS fluorescence detector (Thermo Fisher Scientific, Waltham,
137 MA) using an Acclaim™ VANQUISH C-18 column (2.2 µm, 150 × 2.1 mm; Thermo Fisher
138 Scientific). The mobile phase consisted of two eluents: eluent A (50 mM potassium
139 dihydrogen phosphate in water, adjusted to pH 3.3 with phosphoric acid) and eluent B
140 (70:30 mixture of eluent A and acetonitrile). Separation was achieved using a linear
141 gradient elution program: 80% A/20% B (0-2 min), transitioning to 25% A/75% B (2-10
142 min), followed by 100% B (10-15 min), and returning to initial conditions of 80% A/20% B
143 (15-20 min). The flow rate was maintained at 0.5 mL/min, and the column temperature
144 was held constant at 30°C. Indole derivatives were detected by monitoring native
145 fluorescence using excitation and emission wavelengths of 270 nm and 350 nm,
146 respectively. The following compounds were analyzed: indole, indole-3-acetic acid (IAA),
147 indole-3-propionic acid (IPA), indole-3-aldehyde (I3A), and indole-3-carboxylic acid
148 (I3CA). Compounds were identified through co-chromatography with authentic standards,
149 confirmed by LC-MS, and quantification was performed by integrating peak areas.
150 Method linearity was assessed using standard solutions of each indole derivative
151 prepared at various concentrations. System suitability parameters including retention time
152 stability, peak resolution, and detector response were monitored throughout the analysis.

153 *RNA Isolation for Virulence Factor Expression:* *F.* nucleatum isolates were streaked from
154 frozen stocks and grown in liquid culture from single colonies. Starter cultures were
155 diluted to OD_{600} = 0.3 and used to inoculate three 10 mL cultures per isolate and
156 condition, each treated with either 1 mM indole derivatives (indole, IAA, I3A, I3CA, IPA)
157 or an equivalent volume of DMSO as a control. Cultures were incubated anaerobically for

158 72 h, pooled, and centrifuged at 8000 × g for 5 min. Pellets were resuspended in 1.5 mL
159 chilled lysozyme (0.5 mg/mL; Fisher BioReagents™, Cat# BP535-5), vortexed gently, and
160 incubated at 37°C for ≤5 min. Lysis was performed by adding sodium acetate
161 (Invitrogen™, Cat# AM9740) and SDS (VWR, Cat# 97064-496) to final concentrations of
162 0.1 M and 1%, respectively. After mixing to a gelatinous consistency, an equal volume of
163 Acid-Phenol:Chloroform, pH 4.5 with IAA (25:24:1; Invitrogen™, Cat# AM9720) was
164 added, vortexed, incubated at 65°C for 15 min with intermittent vortexing, then chilled and
165 centrifuged at 18,000 × g (4°C, 20 min). The aqueous layer was transferred to
166 Phasemaker™ tubes (Invitrogen™, Cat# A33248) containing 1/5 volume chloroform,
167 vortexed, and centrifuged at 16,000 × g (4°C, 20 min). The aqueous phase was
168 precipitated with sodium acetate (0.75 M final) and 2x volumes ethanol, then centrifuged
169 at 18,000 × g (4°C, 20 min). Pellets were washed with 80% ethanol, air-dried, and
170 resuspended in nuclease-free water. RNA quality was assessed using a Nanodrop
171 spectrophotometer, and concentrations determined with the Qubit RNA BR Assay Kit
172 (Invitrogen™, Cat# Q10210). Ten micrograms of RNA were treated with TURBO DNA-
173 free™ Kit (Invitrogen™, Cat# AM1906). For cDNA synthesis, 500 ng of RNA was reverse
174 transcribed using the High-Capacity cDNA Reverse Transcription Kit (Applied
175 Biosystems™, Cat# 4368814). cDNA was stored at –20°C.

176 *Real-time quantitative PCR to quantify virulence factor expression:* Real-time quantitative
177 PCR (qPCR) was performed using PowerUp™ SYBR™ Green Master Mix (Thermo
178 Fisher Scientific, Cat. No. A25741) on a QuantStudio 6 Flex Real-Time PCR System
179 (Applied Biosystems). Primers targeting key virulence factors (TnaA, Aid1, FomA, Fap2,
180 FadA, CmpA, RadD, and 16s for reference control) of *F. nucleatum* were either designed
181 in-house or sourced from published literature (Table 2). Prior to experimental analysis,
182 primer efficiency and specificity were evaluated for each target gene using standard
183 curves generated from known concentrations of genomic DNA extracted from the 16 *F.*
184 *nucleatum* isolates. Each experimental reaction was performed in technical triplicates in
185 a total volume of 10 µL containing 5 µL of 2X PowerUp™ SYBR™ Green Master Mix, 250
186 nM of each forward and reverse primer, and 1.5 µL of template DNA at the appropriate
187 dilution. No-template controls were included in each run to monitor potential
188 contamination. Thermal cycling conditions consisted of UDG activation at 50°C for 2
189 minutes, followed by DNA polymerase activation at 95°C for 10 minutes, and 40 cycles
190 of denaturation at 95°C for 15 seconds and annealing/extension at 60°C for 1 minute. A
191 melt curve analysis was performed following amplification by heating samples from 60°C
192 to 95°C at a ramp rate of 0.1°C/second to confirm amplification specificity.

193 *Statistical Methods:* All analyses were conducted in R (v4.3.2) using RStudio
194 (v2024.12.0.467). Detailed statistical analyses are provided in figure legends, with
195 methods implemented as follows: Raw data were processed using the tidyverse package
196 to standardize structure and address missing values. One-way ANOVA (aov()) was used
197 to assess group differences, with significance set at $\alpha = 0.05$. Post-hoc comparisons were
198 performed using Tukey's HSD (TukeyHSD()) to control for family-wise error. Data are
199 shown as means ± SEM unless noted. Plots were generated with ggplot2. For
200 classification, we used Naïve Bayes models (caret, naivebayes) to predict disease status
201 (CRC, Crohn's, Healthy) based on fold-change or binary gene expression. Oral lesion
202 isolates were excluded due to low sample size. Models were trained on 70% of the data

203 and tested on 30%, with 10-fold cross-validation used to assess accuracy, AUC,
204 precision, recall, F1 score, and detection rate. We validated model performance by
205 checking class priors, calculating mutual information and Cramér's V, analyzing feature
206 independence via correlation, and evaluating predictor importance through permutation-
207 based accuracy loss.

208 RESULTS

209 Elevated indole production is a distinctive feature of colorectal cancer-associated 210 *F. nucleatum* isolates

211 Given the role of indole in modulating bacterial virulence, we investigated whether
212 our *F. nucleatum* isolates differ in their capacity to produce indole. We obtained 15 clinical
213 isolates of *F. nucleatum* from patient biopsies representing various disease states (**Table**
214 **1**), along with an oral lesion isolate, ATCC *F. nucleatum subsp. nucleatum* strain 25586
215 heavily cited in the literature. These isolates were categorized into groups based on their
216 disease association: Healthy (3 isolates), Crohn's (6 isolates), CRC (6 isolates), or Oral
217 Lesion (1 isolate). To investigate differences in total indole production profiles, we
218 sampled bacterial cultures throughout the growth phase of *F. nucleatum*. Consistent with
219 existing literature, our *F. nucleatum* isolates displayed varying levels of total indole
220 production **(Figure 1A)**. Heightened indole production was observed at approximately 36
221 hours, suggesting that production primarily occurs during the transition from the
222 exponential to stationary phase. Interestingly, *F. nucleatum* isolates associated with CRC
223 patients exhibited the greatest variance within the disease categories for indole
224 production. However, when categorized by disease association, the CRC isolates
225 exhibited significantly higher indole production across all growth times compared to the
226 other isolates **(Figure 1B)**. Despite variation in total indole production across different
227 growth media, CRC-associated isolates consistently exhibited elevated indole production
228 (**Supplemental Figure 1E**). These findings indicate that elevated indole production is a
229 distinguishing metabolic feature of CRC-associated *F. nucleatum* isolates, potentially
230 contributing to their enhanced virulence and selective advantage within the tumor
231 microenvironment.

232 Disease-associated isolates exhibit elevated production of specific indole 233 derivatives and have distinct indole production profiles.

234 Recent metabolomic analysis revealed differential abundance of tryptophan
235 derivatives—including indole-3-acetic acid (IAA), indole-3-propionic acid (IPA), indole-3-
236 aldehyde (I3A), and indole-3-carboxylic acid (I3CA)—in CRC and adenoma patients
237 compared to healthy controls (20). While overall indole/tryptophan ratios decreased, CRC
238 patients showed elevated levels of specific compounds—I3A and I3CA. Conversely, IPA
239 levels declined in both adenoma and CRC patients. The most intriguing finding was an
240 overall enrichment of *Fusobacteria* in fecal samples from patients with adenomas and
241 CRC. We aimed to investigate whether *F. nucleatum* isolates from diseased environments
242 preferentially produce specific disease-associated indole derivatives compared to strains
243 from healthy environments. The indole production profiles of 16 *F. nucleatum* isolates
244 were characterized using targeted HPLC analysis of spent media collected after 48 hours

of growth, with derivative identification and quantification performed against authenticated standards. *F. nucleatum* isolates from different disease states showed distinct patterns of indole derivative production (**Figure 2A**). The parent indole compound was the predominant indole derivative produced across all isolates. Although all targeted derivatives were detected, most samples had IPA levels below the detection limit. *F. nucleatum* isolates from CRC, Crohn's, and oral lesions trended toward higher production of key indole derivatives—indole, I3A, I3CA, and IAA—relative to healthy isolates, consistent with total indole production data in **Figure 1**. Most notably, the parent indole derivative was significantly elevated in both CRC and Crohn's disease isolates compared to healthy isolates ($p < 0.05$). A similar trend was observed for I3CA and IAA, where disease-associated isolates, particularly those from CRC patients, showed increased production compared to healthy controls ($p < 0.05$). Correlation analysis (**Figure 2B**) revealed distinct associations between specific *F. nucleatum* isolates and their indole derivative profiles. CRC-associated isolates (CC2_6JVN3, CC7_3JVN3C1, SB-CTX47T and SB-CTX3Tcol3) demonstrated strong positive correlations with specific indole derivatives. For the healthy isolates, indole derivative production exhibited a trend toward a negative correlation. The distinct indole production profiles of each isolate suggest a preference for certain indole derivative production over other derivatives. To explore this preference, the ratio of each indole derivative to the parent indole was calculated for each isolate. Examination of individual isolate-to-parent compound ratios (**Figure 2C**) revealed that CRC isolates, particularly CC2_6JVN3, 13 and 14, showed markedly higher I3A ratios (0.7865 and 0.8935, respectively) compared to healthy and oral isolates. Crohn's disease isolates displayed intermediate levels of indole derivatives production, with generally lower ratios than CRC isolates but higher than healthy controls. Isolates grouped by disease showed a more pronounced difference in indole derivative production than isolates grouped by subspecies, suggesting that disease association has a stronger influence on indole production patterns **(Supplemental Figure 2)**. These findings indicate that disease-associated *F. nucleatum* strains—especially those isolated from CRC patients—exhibit distinct metabolic capacities for indole production and can generate the indole derivatives also found in fecal samples from colorectal cancer.

Exposure to indole derivatives alter *F. nucleatum* growth kinetics in a dose-dependent manner without bactericidal effects.

Fecal indole concentrations vary widely from person to person, with levels ranging from 0.3 to 6.64 millimolar (mM) (17). We sought to identify an indole concentration within this range that could be used for exposure without exerting antimicrobial effects.

To assess the impact of increasing indole levels on *F. nucleatum* isolate growth, we continuously monitored the isolates for 72 hours using an automated plate reader while exposing them to increasing indole concentrations. The resulting growth curves were analyzed with the Gompertz mathematical model. The Gompertz model is used to estimate growth parameters such as maximum growth rate, carrying capacity (ODmax), and inflection time, making it useful for comparing bacterial responses to increasing concentrations of indole. This analysis showed that increasing concentrations of indole derivatives restrict maximum growth (OD max) but do not necessarily slow growth rate (μ) or delay inflection time (**Figure 3**). CRC isolates exhibited the highest sensitivity to

289 indole at 2mM concentration, with total population (OD max) reductions of 45% for indole,
290 33% for I3A, 44% for I3CA, 40% for IAA, and 44% for IPA compared to the control (**Figure**
291 **3A and Table 3**). In contrast, Crohn's disease isolates showed substantially lower
292 sensitivity at 2 mM (20% for indole, 15% for I3A, 1% for I3CA, and 0% for both IAA and
293 IPA), as did healthy subject isolates (13% for indole, 0% for I3A, 0% for I3CA, IAA, and
294 IPA). Oral lesion isolates demonstrated minimal sensitivity across all derivatives at 2 mM
295 (0% for indole, 10% for I3A, and 0% for I3CA, IAA, and IPA) (**Figure 3B-D and Tables 4-**
296 **6**). Interestingly, the inflection time—where the growth curve shifts concavity, marking the
297 transition from the exponential phase to a deceleration phase—remained largely
298 unchanged for Crohn's, healthy, and oral isolates within the 0.25 to 1 mM indole range.
299 At 2 mM indole, the isolates exhibited a slight increase in inflection time, suggesting a
300 minimal impact on growth. The CRC isolates exhibited minimal to no variation in inflection
301 time across all concentrations for I3CA, IAA, and IPA treatments. However, indole at 1mM
302 and 2 mM and I3A at 2 mM displayed negative inflection times for the CRC isolates. The
303 negative inflection times in **Table 2** (-21.20, -74.89, -92.97) represent a mathematical
304 anomaly when fitting Gompertz growth models to the bacterial growth data. Negative
305 values likely appear when bacteria begin immediate rapid growth, face severe inhibition
306 **(**e.g chloramphenicol treatment**, Supplemental Figure 3)**, or display atypical growth
307 patterns that don't conform well to the assumptions of the Gompertz model's typical
308 sigmoidal curve shape. Based on the growth patterns, indoles at 2 mM induced
309 modifications to the bacterial growth curve, but the effects differed significantly from
310 severe inhibition. Rather than completely suppressing bacterial proliferation, indole
311 derivatives appear to have altered the fundamental growth dynamics of the bacteria
312 without demonstrating true bactericidal properties. These results suggest indoles may be
313 affecting metabolic pathways or cellular processes predominantly in CRC-associated
314 isolates that influence growth patterns while still allowing bacterial survival and limited
315 proliferation.

316 **Biofilm formation profiles distinguish disease-associated *F. nucleatum* isolates.**

317 While *F. nucleatum* subspecies clearly differ in their ability to form biofilms, we
318 wanted to determine whether isolates from CRC patients have an enhanced propensity
319 to form biofilm. To test this, we monitored biofilm development in all isolates at 12-hour
320 intervals over 72 hours. At 12 hours, several isolates showed minimal biofilm formation,
321 with CC2_3FMU1 (CRC-associated) displaying the highest early biofilm formation
322 **(Figure4A)**. By 36 and 48 hours, when the isolates transitioned from the exponential to
323 the stationary phase, most had reached a stable phase of biofilm development, with
324 EAVG002-7_1 (Crohn's), SB-CTX3Tcol3 (CRC), and EAVG_014 (Healthy) consistently
325 forming the most robust biofilms, while isolates such as CC2_6JVN3 (CRC), CC53 (CRC)
326 and CC7_3JVN3C1 (CRC) produced minimal biofilm **(Supplemental Figure 4A)**. By 72
327 hours, a clear distinction emerged between high and low biofilm-forming isolates
328 **(Supplemental Figure 4B)**, with the high biofilm formers predominantly associated with
329 Crohn's disease **(Figure 4B)**. Interestingly, the CRC-associated isolates generally
330 exhibited the lowest baseline biofilm formation, with the notable exception of SB-
331 CTX3Tcol3, which was among the strongest biofilm producers. Collectively, these data
332 demonstrate that *F. nucleatum* isolates exhibit considerable variability in biofilm formation
333 capability, paralleling their diverse indole derivative production profiles.

334 **Biofilm formation by CRC-associated *F. nucleatum* isolates is positively correlated**
335 **with total indole production.**

336 Bacteria are known to use indole production and biofilm formation as stress
337 responses, increasing their survival in hostile environments. We sought to determine if
338 total indole production corresponds with biofilm formation among our disease categories.
339 This relationship was examined through linear correlation analysis comparing total indole
340 against biofilm formation at defined intervals throughout the growth cycle from our two
341 independent experiments. *F. nucleatum* isolates produce indole and form biofilms upon
342 entering the stationary phase (at 36- and 48-hours), a phase triggered by cellular stress
343 due to reduced nutrient availability. Looking at this 36-hour time point, a negative
344 correlation between total indole production and biofilm formation was observed in healthy-
345 associated isolates (R^2 = 0.72, $p < 0.001$) **(Figure 5C)**. Crohn's-associated isolates
346 showed a weaker and non-significant negative correlation (R^2 = 0.04, p = 0.051) **(Figure**
347 **5B and D)**. However, a strong positive correlation was observed for the CRC-associated
348 isolates (R^2 = 0.5, $p < 0.001$) at this time point **(Figure 5A)**. At 48 hours, the negative
349 correlation between total indole production and biofilm formation strengthened for
350 healthy-associated isolates (R^2 = 0.88, $p < 0.001$). Crohn's-associated isolates continued
351 to show a moderate negative correlation (R^2 = 0.10, $p < 0.001$) and the oral associated
352 isolates again exhibited no significant correlation ($R^2 < 0.01$, p = 1). However, it should
353 be noted that there is only one oral isolate represented in this study. The positive
354 correlation between indole production and biofilm formation at 48 hours strengthened for
355 CRC-associated isolates (R^2 = 0.70, $p < 0.001$). These results indicate that total indole
356 production and biofilm formation are inversely related in healthy-associated and Crohn's-
357 associated isolates, while CRC-associated isolates show a positive correlation at both 36
358 and 48 hours. Thus, total indole production may act as a biofilm-promoting signal in the
359 tumor microenvironment, potentially enhancing bacterial persistence and pathogenicity in
360 colorectal cancer.

361 **Exposure to indole derivatives significantly diminish biofilm formation in CRC-**
362 **associated *F. nucleatum* isolates.**

363 To determine whether indole derivatives influence biofilm formation, bacterial
364 isolates were cultured with increasing concentrations of the derivatives, and biofilm
365 formation was quantified after a 72-hour incubation period. Administration of exogenous
366 indole and its derivatives (I3A, I3CA, IAA, and IPA) resulted in distinct biofilm formation
367 responses that varied based on the disease association **(Figure 6)**. CRC-associated
368 isolates demonstrated significant biofilm inhibition at higher concentrations of several
369 indole derivatives. Indole treatment at 2.0 mM reduced biofilm formation by approximately
370 25% ($p<0.01$) compared to untreated controls. Similarly, I3CA and IAA at 2.0 mM
371 substantially inhibited biofilm formation by approximately 40% ($p<0.01$). Interestingly, I3A
372 exhibited a biphasic response in CRC isolates, with enhanced biofilm formation
373 (approximately 25% increase) at 0.5 mM followed by statistically significant inhibition at
374 higher concentrations ($p<0.01$). Healthy-associated isolates exhibited variable responses
375 with modest effects overall. A slight but significant increase in biofilm formation was
376 observed at 1.0 mM indole ($p<0.05$), while other derivatives showed minimal impact
377 across most concentrations. Unlike CRC and oral isolates, healthy-derived strains

demonstrated neither strong stimulation nor inhibition patterns, suggesting a more neutral sensitivity to indole signaling. Crohn's disease-associated isolates showed intermediate responses with greater variability. The effects were generally less pronounced than those observed in CRC or oral isolates, with most treatments resulting in slight, non-significant deviations from baseline. I3CA at 2 mM showed moderate inhibitory effects, but did not reach statistical significance for the Crohn's associated isolates. The orally derived *F. nucleatum* isolate displayed a consistent stimulatory response to indole derivatives across all tested concentrations. This effect was most prominent at lower concentrations (0.5-1.0 mM), with statistical significance ($p<0.05$) observed for indole, I3A, I3CA, and IAA treatments. Even at higher concentrations (2.0 mM), where CRC isolates showed inhibition, oral isolates-maintained biofilm levels above untreated controls. The most pronounced stimulation was observed with indole at 1.0 mM and I3CA at 0.5 mM, both inducing approximately 20% enhancement in biofilm formation. These results reveal that indole and its derivatives modulate *F. nucleatum* biofilm formation in a disease context-dependent manner, with CRC isolates being particularly susceptible to biofilm inhibition at higher indole concentrations, while our single oral isolate demonstrated enhanced biofilm formation across all concentrations tested.

Indole derivatives elicit distinct virulence expression patterns in *F. nucleatum* based on isolate origin and disease-association.

To assess indole derivative influence on bacterial virulence potential, we analyzed transcriptional alterations in key virulence-associated genes (tnaA, FomA, FadA, Fap2, RadD, CmpA, and Aid1) across our *F. nucleatum* isolates following indole exposure. Exposure to indole or indole derivatives elicited markedly distinct transcriptional responses among the *F. nucleatum* isolates analyzed. RT-qPCR analysis revealed that the expression patterns of key virulence-associated genes varied not only with the specific indole derivative but also in an isolate-dependent manner (**Figure 7A**). Specifically, aid1 showed a diverse expression profile with significantly higher expression in isolates EAVG_029, EAVG_030, and EAVG002-7_1 under indole exposure, yet was significantly reduced in CC2_3FMU1 and CC2_6JVN3. Genes involved in adhesion and immune modulation, including FomA, RadD, and FadA, also exhibited heterogeneous responses. Notably, FadA expression was decreased across all treatments in *vincentii*, while being increased in several tumor-associated isolates (CC53, CC7_3JVN3C1, and SB-CTX3Tcol3). Fap2 expression was generally low or undetectable, yet select isolates (EAVG_012, EAVG_029, and CC53) showed significant expression in response to certain indole derivatives. Examining the disease-association expression patterns, FomA showed opposite responses to indole—reduced in healthy isolates and increased in most CRC-associated isolates. To better assess whether indole-induced responses differed by disease association, we used a naïve Bayes classification model to test if indole-induced expression patterns could predict disease origin for each isolate **(Figure 7B)**. Using the raw fold change data and the gene direction threshold, the naïve Bayes model was able to predict disease association with high accuracy (74% and $P<2.2e-16$, 76% and $P<2e-16$, respectively). The two models also exhibited a strong true positive rate, suggesting the models were very good at correctly identifying positive cases (AUC = 0.9019, AUC = 0.9221 respectively). Together, these results suggest that indole derivatives modulate *F.*

nucleatum virulence factor expression in a strain-dependent manner, with isolates from the same disease environment showing similar responses to indole.

Naïve Bayes posterior probabilities and feature importance reveal class-specific predictive confidence based on gene expression direction and fold change.

To assess the model's confidence in classifying samples based on gene fold-change and directionality, we examined the posterior probabilities of true positive predictions across the three disease classes: CRC, Crohn's, and Healthy **(Figure 8A)**. Posterior probability reflects the naïve Bayes model's confidence, with values near 1 indicating high certainty and values near 1/3 (the random chance threshold in a three-class model) indicating low confidence. The gene direction model **(Figure 8A, left)** accurately classifies CRC, Crohn's, and Healthy isolates, showing strong confidence across groups (CRC avg = 0.662, Crohn's avg = 0.644, Healthy avg = 0.757). Healthy samples had the highest classification accuracy and lowest false positive rates (avg wrong CRC = 0.196, avg wrong Crohn's = 0.0468). Misclassifications typically fell below the 1/3 threshold (e.g., true CRC: avg wrong Crohn's = 0.271, avg wrong Healthy = 0.067; true Crohn's: avg wrong CRC = 0.292, avg wrong Healthy = 0.064), indicating the model appropriately expressed uncertainty when incorrect. The gene fold model **(Figure 8B, left)** also performed well, particularly for Crohn's (avg correct = 0.890; avg wrong Healthy = 0.0512, avg wrong CRC = 0.0593), and showed moderate confidence for CRC (avg correct = 0.697; avg wrong Crohn's = 0.286, avg wrong Healthy = 0.0167). However, it performed less reliably for Healthy samples, with more variable predictions (avg correct = 0.387; avg wrong Crohn's = 0.323, avg wrong CRC = 0.290). Nevertheless, gene directionality data appeared to be more effective at predicting all disease classes compared to other fold data. These data suggest that indole-induced virulence factor expression response may be specific to the isolate's disease origin. To identify which gene features most strongly influence model performance, we applied Leave-One-Feature-Out (LOFO) importance—also known as permutation importance—which quantifies the individual contribution of each feature by measuring the change in model accuracy when it is removed. In the directionality model, FomA and RadD caused the greatest drop in accuracy when removed **(Figure 8A, right)**, indicating their high predictive importance, while aid1 emerged as the most influential feature in the fold-change model **(Figure 8B, right)**. Taken together, these findings suggest that indole may drive the expression of specific virulence factors in a manner tailored to the environmental niche.

DISCUSSION

A key unanswered question is how *F. nucleatum* transitions from an oral commensal organism to a virulent intestinal pathogen, and which molecular mechanisms drive its dual role in host health. *F. nucleatum* exhibits significant heterogeneity, with strains categorized into subspecies based on genomic and physiological analyses (21–28)—so pronounced that reclassification into separate species has been proposed (29). At the subspecies level, *F. nucleatum* subspecies *animalis* specifically correlates with increased CRC-specific mortality and distinctive somatic gene mutations (30). Recently, subspecies *animalis* has been subdivided into two distinct clades characterized by the

465 differential presence of key virulence factors (31), with clade Fna C2—which notably
466 possess fap2 and cmpA genes—were found to be significantly enriched within biofilm-
467 positive CRC tumor microenvironments (11). Given that specific virulence factors in *F.*
468 *nucleatum* serve as biological markers of its association with CRC, elucidating the
469 mechanisms that regulate the expression of these virulence factors is essential to
470 comprehend the complex community interactions between this organism and disease
471 pathology. Our study offers new insight by highlighting an underexplored virulence
472 mechanism. To our knowledge, this is the first comparative analysis of indole production
473 across clinical *F. nucleatum* isolates, revealing that indole derivatives may modulate
474 virulence in a disease- and environment-specific manner through modulation of biofilm
475 formation and virulence factor expression. This is supported by our data showing distinct
476 indole production profiles that correlate with disease association and differential
477 responses to indole exposure.

478 The human gut contains numerous signals that regulate host-microbiota and
479 microbiota-microbiota interactions to maintain GI homeostasis (32–36). Microbiota-
480 derived tryptophan metabolites, such as indole, support intestinal barrier function and
481 modulate host immunity (9,37), including direct effects on the tumor immune
482 microenvironment (38,39). These effects vary by indole species: indole-3-acetic acid
483 (IAA) suppresses immune responses in pancreatic cancer by activating the aryl
484 hydrocarbon receptor (AhR) in tumor-associated macrophages, reducing $CD8^+$ T cell
485 activation (39). Supplementation with IAA or IAA-producing bacteria alleviates colitis in
486 mice, while loss of AhR or reduced IAA levels (such as from a high-fat diet) worsens
487 inflammation and barrier dysfunction (40). Certain indole derivatives exhibit dose-
488 dependent bidirectional effects on host cells, with indole-3-acetaldehyde (IAAD) inhibiting
489 cell proliferation and inducing apoptosis at low concentrations, thereby preventing CRC
490 development, while at higher concentrations (>25 μmol/L), it promotes epithelial-
491 mesenchymal transition and invasion in CRC cells (41). Similarly, indole-3-aldehyde (I3A)
492 reduces colitis induced inflammation and helps restore intestinal epithelial barrier function
493 (42), in part by activating AhR, which can also promote IL-22 secretion (43). While IL-22
494 is protective in some contexts, it can promote tumor growth in colorectal cancer (44),
495 highlighting the context-dependent roles of indole derivatives.

496 Metabolism of tryptophan into indoles is a key metabolic pathway commonly
497 altered in gastrointestinal diseases (20,45–47). Specifically, in multiple IBD and CRC
498 studies tryptophan and indole levels are significantly different from controls, with higher
499 fecal tryptophan but lower serum tryptophan levels suggesting possible malabsorption
500 (48–53). A meta-analysis of fecal samples revealed elevated tryptophan metabolism and
501 decreased tryptophan biosynthesis in tumor samples compared to non-tumor controls,
502 suggesting possible increased indole production in the tumor microenvironment (54–56)
503 (**Supplemental Figure 9**). Due to the established enrichment of *F. nucleatum* in CRC
504 tissue (1,2,11,31), we investigated whether CRC-associated *F. nucleatum* isolates could
505 contribute to elevated tryptophan metabolism. Comparative analysis revealed that CRC-
506 associated *F. nucleatum* isolates produced significantly higher levels of total indole than
507 isolates from other disease groups, suggesting a potential link between CRC and *F.*
508 *nucleatum*-mediated indole production. Supporting this, indole derivatives (indole, I3A,
509 I3CA) enriched in CRC fecal samples (20) positively correlated with indole levels in CRC-

510 derived isolates. Notably, I3A—elevated in CRC samples—was preferentially produced
511 by three CRC-associated *F. nucleatum* isolates (CC2_6JVN3, SB-CTX47T, SB-
512 CTX3Tcol3). These findings suggest a potential metabolic adaptation in CRC-associated
513 isolates toward increased indole production, likely driven by microenvironmental cues.

514 Fecal indole levels range from 0.3–6.6 mM (17), with *in vitro* studies showing
515 similar concentrations (0.5–5 mM) (57). At low levels (0.5–1 mM), indole modulates *E.*
516 *coli* virulence by affecting biofilm formation, gene expression, and stress responses
517 (58,59), while higher levels (4–5 mM) inhibit growth and division (60). We examined
518 whether low concentrations could similarly modulate *F. nucleatum* growth kinetics without
519 exerting antimicrobial effects. At 0.25–2 mM, indole primarily reduced carrying capacity
520 (OD max) without altering inflection time, with CRC isolates showing the greatest
521 sensitivity as compared to other non-CRC isolates. Overall, minimal growth effects at 1
522 mM across all derivatives suggest phenotypic modulation rather than direct toxicity.

523 Biofilm analysis revealed distinct high and low biofilm-forming isolates. SB-
524 CTX3Tcol3 (CRC) and EAVG002-7_1 (Crohn's) peaked at 36 hours, identifying them as
525 strong biofilm producers and suggesting potential for persistent virulence. EAVG002-7_1,
526 part of a specific *F. nucleatum* clade associated with CRC (31), has been shown to induce
527 colonic tumors in mouse models where most isolates fail to colonize (61,62). Interestingly,
528 Crohn's-associated isolates were the strongest biofilm formers, while only CC2_3FMU1
529 and SB-CTX3Tcol3 showed strong formation among CRC isolates. When analyzing the
530 36 and 48-hour time points—which mark the beginning of stationary phase when indole
531 production and biofilm formation are typically activated—only CRC isolates demonstrated
532 this positive correlation with total indole production. These results suggest that CRC-
533 associated *F. nucleatum* isolates possess a unique metabolic relationship between total
534 indole signaling and biofilm development that distinguishes them from non-CRC isolates,
535 which may provide a fitness advantage in the malignant microenvironment.

536 Recent studies in the field have highlighted virulence clades of *F. nucleatum* based
537 on the presence and absence of certain virulence factors, potentially serving as biological
538 markers of its association with CRC (31). During active invasion, *F. nucleatum*
539 reprograms its metabolic and functional pathways to adapt to the host-imposed
540 environment, marked by the upregulation of metabolic processes, quorum sensing, and
541 amino acid metabolism (63). In addition, *F. nucleatum* switches it's the expression profile
542 during the transition from planktonic to the biofilm phase, another pathway mediated by
543 upregulation of amino acid metabolism (64). These data support the concept that *F.*
544 *nucleatum* tailors its metabolic and transcriptional profiles in response to environmental
545 cues. However, the transcriptional regulation of *F. nucleatum* in response to specific
546 indole derivatives, compounds found to be abundant in the CRC environment (20),
547 remains poorly understood. Analysis of key virulence factors (Aid1, FomA, Fap2, FadA,
548 CmpA, and RadD) following exposure to five indole derivatives (indole, I3A, I3CA, IAA,
549 and IPA) revealed distinct, isolate-specific transcriptional responses. Interestingly,
550 disease-specific responses were particularly evident for FomA: most CRC-associated
551 isolates exhibited increased FomA expression across nearly all indole treatments,
552 whereas most health-associated isolates showed a corresponding decrease in
553 expression. This disease-specific response presents an opportunity to selectively target

554 CRC-associated *F. nucleatum* isolates by exploiting their heightened FomA expression
555 in response to indole. Our lab has developed guided antimicrobial peptides (gAMPs)
556 against FomA , and these findings may enhance their efficacy by enabling more precise
557 eradication of pathogenic isolates linked to CRC through combination of indole and gAMP
558 treatment.

559 To further validate the disease-specific expression patterns of virulence factors in
560 response to indole derivatives, we employed a Naïve Bayes classification model trained
561 on indole-induced expression profiles (gene directionality and fold expression data), with
562 the objective of predicting the disease association of each isolate. Both models accurately
563 classified CRC, Crohn's, and healthy isolates (fold expression: 74%, $P < 2.2e-16$;
564 directionality: 76%, $P < 2e-16$). These findings suggest that both indole production and
565 indole sensitivity are shaped by environmental pressures, contributing to niche-specific
566 adaptation in *F. nucleatum*. Contrary to our initial hypothesis that indole derivatives would
567 enhance all aspects of *F. nucleatum* virulence, CRC-associated isolates showed reduced
568 biofilm formation alongside increased virulence gene expression. A similar inverse
569 relationship has been reported in *P. aeruginosa*, where disruption of the Entner-Doudoroff
570 pathway decreased biofilm but increased lethality and immune activation in infection
571 models (66). Indole exposure may likewise trigger metabolic pathways that suppress
572 biofilm while enhancing immune resilience in *F. nucleatum*. This response appears niche-
573 specific, with oral isolates rapidly forming biofilms under distinct environmental pressures,
574 while CRC isolates suppress biofilm formation in favor of niche-specific virulence
575 behaviors. Further transcriptomic and proteomic analyses—particularly during active
576 invasion of oral versus colorectal cancer cells—are needed to define the transcriptional
577 programs driving these niche-specific behaviors.

578 Despite the novel insights presented, this study has several notable limitations. All
579 experiments were performed in monoculture, lacking the polymicrobial and host-
580 interactive context of the gut or tumor microenvironment, where microbial crosstalk and
581 host interactions significantly influence bacterial behavior. The inclusion of only a single
582 oral isolate limits conclusions about niche-specific responses. Although correlations
583 between indole production, biofilm formation, and virulence gene expression are
584 compelling, underlying regulatory mechanisms remain uncharacterized. Additionally, the
585 positive correlation between total indole levels and biofilm formation in CRC-associated
586 isolates suggests the existence of other, untested indole derivatives that may enhance
587 biofilm formation in these strains—contrasting with the derivatives examined in this study,
588 which were associated with reduced biofilm production. The use of rich artificial media
589 further reduces physiological relevance, and the absence of host models restricts
590 translational applicability. It is likely isolate behavior may differ in the presence of indoles
591 within a more biologically relevant polymicrobial fecal environment or during active host
592 cell invasion—conditions currently under investigation in our lab.

593 The differential responses to indole exposure among *F. nucleatum* isolates from
594 CRC, Crohn's disease, oral sites, and healthy individuals underscore the importance of
595 investigating indole's role in disease pathogenesis and persistence. These findings
596 suggest potential for targeted therapeutic strategies in colorectal, where inhibiting biofilm
597 formation or indole production could reduce pathogenicity (67). Moreover, the use of

598 gAMPs targeting virulence factors that are consistently upregulated in CRC-associated
599 isolates following indole exposure—such as FomA—may enhance the selective
600 eradication of highly virulent strains. Future research should examine how indole and its
601 derivatives simultaneously modulate both bacterial and host transcriptomes during active
602 infection and explore how these metabolites shape microbial community dynamics in
603 polymicrobial environments.

604 **References**

605 1. Kostic AD, Gevers D, Pedamallu CS, Michaud M, Duke F, Earl AM, et al. Genomic
606 analysis identifies association of Fusobacterium with colorectal carcinoma. Genome
607 Res. 2012 Feb;22(2):292–8.

608 2. Castellarin M, Warren RL, Freeman JD, Dreolini L, Krzywinski M, Strauss J, et al.
609 Fusobacterium nucleatum infection is prevalent in human colorectal carcinoma.
610 Genome Res. 2012 Feb;22(2):299–306.

611 3. Umana A, Sanders BE, Yoo CC, Casasanta MA, Udayasuryan B, Verbridge SS, et
612 al. Reevaluating the Fusobacterium Virulence Factor Landscape [Internet]. bioRxiv;
613 2019 [cited 2024 Oct 17]. p. 534297. Available from:
614 https://www.biorxiv.org/content/10.1101/534297v1

615 4. Kaplan A, Kaplan CW, He X, McHardy I, Shi W, Lux R. Characterization of aid1, a
616 novel gene involved in Fusobacterium nucleatum interspecies interactions. Microb
617 Ecol. 2014 Aug;68(2):379–87.

618 5. Zhang L, Leng XX, Qi J, Wang N, Han JX, Tao ZH, et al. The adhesin RadD
619 enhances Fusobacterium nucleatum tumour colonization and colorectal
620 carcinogenesis. Nat Microbiol. 2024 Sep;9(9):2292–307.

621 6. Abed J, Emgård JEM, Zamir G, Faroja M, Almogy G, Grenov A, et al. Fap2
622 Mediates Fusobacterium nucleatum Colorectal Adenocarcinoma Enrichment by
623 Binding to Tumor-Expressed Gal-GalNAc. Cell Host Microbe. 2016 Aug
624 10;20(2):215–25.

625 7. Rubinstein MR, Wang X, Liu W, Hao Y, Cai G, Han YW. Fusobacterium nucleatum
626 promotes colorectal carcinogenesis by modulating E-cadherin/β-catenin signaling
627 via its FadA adhesin. Cell Host Microbe. 2013 Aug 14;14(2):195–206.

628 8. Ma CT, Luo HS, Gao F, Tang QC, Chen W. Fusobacterium nucleatum promotes the
629 progression of colorectal cancer by interacting with E-cadherin. Oncol Lett. 2018
630 Aug 1;16(2):2606–12.

631 9. Bansal T, Alaniz RC, Wood TK, Jayaraman A. The bacterial signal indole increases
632 epithelial-cell tight-junction resistance and attenuates indicators of inflammation.
633 Proc Natl Acad Sci. 2010 Jan 5;107(1):228–33.

634 10. Dejea CM, Wick EC, Hechenbleikner EM, White JR, Mark Welch JL, Rossetti BJ, et
635 al. Microbiota organization is a distinct feature of proximal colorectal cancers. Proc
636 Natl Acad Sci U S A. 2014 Dec 23;111(51):18321–6.

637 11. Queen J, Cing Z, Minsky H, Nandi A, Southward T, Ferri J, et al. Fusobacterium
638 nucleatum is enriched in invasive biofilms in colorectal cancer. bioRxiv. 2025 Jan
639 1;2024.12.30.630810.

640 12. Sasaki-Imamura T, Yano A, Yoshida Y. Production of Indole from l-Tryptophan and
641 Effects of These Compounds on Biofilm Formation by Fusobacterium nucleatum
642 ATCC 25586. Appl Environ Microbiol. 2010 Jul;76(13):4260–8.

643 13. Lee JH, Lee J. Indole as an intercellular signal in microbial communities. FEMS
644 Microbiol Rev. 2010 Jul 1;34(4):426–44.

645 14. Wang G, Fan Y, Zhang G, Cai S, Ma Y, Yang L, et al. Microbiota-derived indoles
646 alleviate intestinal inflammation and modulate microbiome by microbial cross-
647 feeding. Microbiome. 2024 Mar 19;12(1):59.

648 15. Sakanaka A, Kuboniwa M, Shimma S, Alghamdi SA, Mayumi S, Lamont RJ, et al.
649 Fusobacterium nucleatum Metabolically Integrates Commensals and Pathogens in
650 Oral Biofilms. mSystems. 2022 Jul 19;7(4):e00170-22.

651 16. Abed J, Maalouf N, Manson AL, Earl AM, Parhi L, Emgård JEM, et al. Colon
652 Cancer-Associated Fusobacterium nucleatum May Originate From the Oral Cavity
653 and Reach Colon Tumors via the Circulatory System. Front Cell Infect Microbiol
654 [Internet]. 2020 [cited 2022 Nov 30];10. Available from:
655 https://www.frontiersin.org/articles/10.3389/fcimb.2020.00400

656 17. Darkoh C, Chappell C, Gonzales C, Okhuysen P. A rapid and specific method for
657 the detection of indole in complex biological samples. Appl Environ Microbiol. 2015
658 Dec;81(23):8093–7.

659 18. Tuomola M, Vahva M, Kallio H. High-Performance Liquid Chromatography
660 Determination of Skatole and Indole Levels in Pig Serum, Subcutaneous Fat, and
661 Submaxillary Salivary Glands. J Agric Food Chem. 1996 Jan 1;44(5):1265–70.

662 19. Kema IP, Meijer WG, Meiborg G, Ooms B, Willemse PHB, De Vries EGE. Profiling
663 of Tryptophan-related Plasma Indoles in Patients with Carcinoid Tumors by
664 Automated, On-Line, Solid-Phase Extraction and HPLC with Fluorescence
665 Detection. Clin Chem. 2001 Oct 1;47(10):1811–20.

666 20. Sun XZ, Zhao DY, Zhou YC, Wang QQ, Qin G, Yao SK. Alteration of fecal
667 tryptophan metabolism correlates with shifted microbiota and may be involved in
668 pathogenesis of colorectal cancer. World J Gastroenterol. 2020 Dec 7;26(45):7173–
669 90.

670 21. Loesche WJ, Gibbons RJ. Amino acid fermentation by Fusobacterium nucleatum.
671 Arch Oral Biol. 1968 Feb;13(2):191–202.

672 22. Dzink JL, Socransky SS. Amino acid utilization by Fusobacterium nucleatum grown
673 in a chemically defined medium. Oral Microbiol Immunol. 1990 Jun;5(3):172–4.

674 23. Suchett-Kaye G, Décoret D, Barsotti O. Clonal analysis by ribotyping of
675 Fusobacterium nucleatum isolates obtained from healthy young adults with optimal
676 plaque control. J Periodontal Res. 1998 May;33(4):179–86.

677 24. Thurnheer T, Guggenheim B, Gruica B, Gmür R. Infinite Serovar and Ribotype
678 Heterogeneity Among Oral *Fusobacterium nucleatum* Strains? Anaerobe. 1999 Apr
679 1;5(2):79–92.

680 25. Morris ML, Andrews RH, Rogers AH. Investigations of the Taxonomy and
681 Systematics of Fusobacterium nucleatum Using Allozyme Electrophoresis. Int J Syst
682 Evol Microbiol. 1997;47(1):103–10.

683 26. Strauss J, White A, Ambrose C, McDonald J, Allen-Vercoe E. Phenotypic and
684 genotypic analyses of clinical *Fusobacterium nucleatum* and *Fusobacterium*
685 *periodonticum* isolates from the human gut. Anaerobe. 2008 Dec 1;14(6):301–9.

686 27. Krieger M, Guo M, Merritt J. Reexamining the role of Fusobacterium nucleatum
687 subspecies in clinical and experimental studies. Gut Microbes. 16(1):2415490.

688 28. Krieger M, AbdelRahman YM, Choi D, Palmer EA, Yoo A, McGuire S, et al.
689 Stratification of Fusobacterium nucleatum by local health status in the oral cavity
690 defines its subspecies disease association. Cell Host Microbe. 2024 Apr
691 10;32(4):479-488.e4.

692 29. Kook JK, Park SN, Lim YK, Cho E, Jo E, Roh H, et al. Genome-Based
693 Reclassification of Fusobacterium nucleatum Subspecies at the Species Level. Curr
694 Microbiol. 2017 Oct;74(10):1137–47.

695 30. Borozan I, Zaidi SH, Harrison TA, Phipps AI, Zheng J, Lee S, et al. Molecular and
696 pathology features of colorectal tumors and patient outcomes are associated with
697 Fusobacterium nucleatum and its subspecies animalis. Cancer Epidemiol Biomark
698 Prev Publ Am Assoc Cancer Res Cosponsored Am Soc Prev Oncol. 2022
699 Jan;31(1):210–20.

700 31. Zepeda-Rivera M, Minot SS, Bouzek H, Wu H, Blanco-Míguez A, Manghi P, et al. A
701 distinct Fusobacterium nucleatum clade dominates the colorectal cancer niche.
702 Nature. 2024 Apr;628(8007):424–32.

703 32. Wang T, Zheng X, Ji H, Wang TL, Xing XH, Zhang C. Dynamics of transcription–
704 translation coordination tune bacterial indole signaling. Nat Chem Biol. 2020
705 Apr;16(4):440–9.

706 33. Cameron E, Sperandio V. Frenemies: Signaling and nutritional integration in
707 pathogen-microbiota-host interactions. Cell Host Microbe. 2015 Sep 9;18(3):275–84.

708 34. Kumar A, Sperandio V. Indole Signaling at the Host-Microbiota-Pathogen Interface.
709 mBio. 10(3):e01031-19.

710 35. Bäumler AJ, Sperandio V. Interactions between the microbiota and pathogenic
711 bacteria in the gut. Nature. 2016 Jul;535(7610):85–93.

712 36. Falà AK, Álvarez-Ordóñez A, Filloux A, Gahan CGM, Cotter PD. Quorum sensing in
713 human gut and food microbiomes: Significance and potential for therapeutic
714 targeting. Front Microbiol [Internet]. 2022 Nov 25 [cited 2025 Feb 18];13. Available
715 from:
716 https://www.frontiersin.org/journals/microbiology/articles/10.3389/fmicb.2022.100218
717 5/full

718 37. Wang D, Ding X, Rather PN. Indole Can Act as an Extracellular Signal in
719 Escherichia coli. J Bacteriol. 2001 Jul;183(14):4210–6.

720 38. Bender MJ, McPherson AC, Phelps CM, Pandey SP, Laughlin CR, Shapira JH, et al.
721 Dietary tryptophan metabolite released by intratumoral Lactobacillus reuteri
722 facilitates immune checkpoint inhibitor treatment. Cell. 2023 Apr 27;186(9):1846-
723 1862.e26.

724 39. Hezaveh K, Shinde RS, Klötgen A, Halaby MJ, Lamorte S, Ciudad MT, et al.
725 Tryptophan-derived microbial metabolites activate the aryl hydrocarbon receptor in
726 tumor-associated macrophages to suppress anti-tumor immunity. Immunity. 2022
727 Feb 8;55(2):324-340.e8.

728 40. Li M, Ding Y, Wei J, Dong Y, Wang J, Dai X, et al. Gut microbiota metabolite indole-
729 3-acetic acid maintains intestinal epithelial homeostasis through mucin sulfation. Gut
730 Microbes. 16(1):2377576.

731 41. Dai Z, Deng KL, Wang XM, Yang DX, Tang CL, Zhou YP. Bidirectional effects of the
732 tryptophan metabolite indole-3-acetaldehyde on colorectal cancer. World J
733 Gastrointest Oncol. 2024 Jun 15;16(6):2697–715.

734 42. Wang M, Guo J, Hart AL, Li JV. Indole-3-Aldehyde Reduces Inflammatory
735 Responses and Restores Intestinal Epithelial Barrier Function Partially via Aryl
736 Hydrocarbon Receptor (AhR) in Experimental Colitis Models. J Inflamm Res. 2023
737 Dec 6;16:5845–64.

738 43. Zelante T, Iannitti RG, Cunha C, De Luca A, Giovannini G, Pieraccini G, et al.
739 Tryptophan catabolites from microbiota engage aryl hydrocarbon receptor and
740 balance mucosal reactivity via interleukin-22. Immunity. 2013 Aug 22;39(2):372–85.

741 44. Strauss J, Kaplan GG, Beck PL, Rioux K, Panaccione R, DeVinney R, et al. Invasive
742 potential of gut mucosa-derived fusobacterium nucleatum positively correlates with
743 IBD status of the host. Inflamm Bowel Dis. 2011 Sep 1;17(9):1971–8.

744 45. Papadimitriou N, Gunter MJ, Murphy N, Gicquiau A, Achaintre D, Brezina S, et al.
745 Circulating tryptophan metabolites and risk of colon cancer: results from case-
746 control and prospective cohort studies. Int J Cancer. 2021 Nov 1;149(9):1659–69.

747 46. Liu Y, Pei Z, Pan T, Wang H, Chen W, Lu W. Indole metabolites and colorectal
748 cancer: Gut microbial tryptophan metabolism, host gut microbiome biomarkers, and
749 potential intervention mechanisms. Microbiol Res. 2023 Jul 1;272:127392.

750 47. Venkateswaran N, Lafita-Navarro MC, Hao YH, Kilgore JA, Perez-Castro L,
751 Braverman J, et al. MYC promotes tryptophan uptake and metabolism by the
752 kynurenine pathway in colon cancer. Genes Dev. 2019 Sep 1;33(17–18):1236–51.

753 48. Bosch S, de Meij TGJ, de Boer NK. Altered Tryptophan Levels in Patients With
754 Inflammatory Bowel Disease Owing to Colonic Leakage, Metabolism, or
755 Malabsorption? Gastroenterology. 2018 May 1;154(6):1855–6.

756 49. Cheng J, Jin H, Hou X, Lv J, Gao X, Zheng G. Disturbed tryptophan metabolism
757 correlating to progression and metastasis of esophageal squamous cell carcinoma.
758 Biochem Biophys Res Commun. 2017 May 6;486(3):781–7.

759 50. Nikolaus S, Schulte B, Al-Massad N, Thieme F, Schulte DM, Bethge J, et al.
760 Increased Tryptophan Metabolism Is Associated With Activity of Inflammatory Bowel
761 Diseases. Gastroenterology. 2017 Dec;153(6):1504-1516.e2.

762 51. Wang S, van Schooten FJ, Jin H, Jonkers D, Godschalk R. The Involvement of
763 Intestinal Tryptophan Metabolism in Inflammatory Bowel Disease Identified by a
764 Meta-Analysis of the Transcriptome and a Systematic Review of the Metabolome.
765 Nutrients. 2023 Jun 26;15(13):2886.

766 52. Bustamante S, Yau Y, Boys V, Chang J, Paramsothy S, Pudipeddi A, et al.
767 Tryptophan Metabolism “Hub” Gene Expression Associates with Increased
768 Inflammation and Severe Disease Outcomes in COVID-19 Infection and
769 Inflammatory Bowel Disease. Int J Mol Sci. 2022 Nov 26;23(23):14776.

770 53. Crotti S, D’Angelo E, Bedin C, Fassan M, Pucciarelli S, Nitti D, et al. Tryptophan
771 metabolism along the kynurenine and serotonin pathways reveals substantial
772 differences in colon and rectal cancer. Metabolomics. 2017 Dec;13(12):148.

773 54. Feng Q, Liang S, Jia H, Stadlmayr A, Tang L, Lan Z, et al. Gut microbiome
774 development along the colorectal adenoma–carcinoma sequence. Nat Commun.
775 2015 Mar 11;6(1):6528.

776 55. Vogtmann E, Hua X, Zeller G, Sunagawa S, Voigt AY, Hercog R, et al. Colorectal
777 Cancer and the Human Gut Microbiome: Reproducibility with Whole-Genome
778 Shotgun Sequencing. PLoS ONE. 2016 May 12;11(5):e0155362.

779 56. Zeller G, Tap J, Voigt AY, Sunagawa S, Kultima JR, Costea PI, et al. Potential of
780 fecal microbiota for early-stage detection of colorectal cancer. Mol Syst Biol. 2014
781 Nov 28;10(11):766.

782 57. Gaimster H, Summers D. Regulation of Indole Signalling during the Transition of E.
783 coli from Exponential to Stationary Phase. PLoS ONE. 2015 Sep 2;10(9):e0136691.

784 58. Hirakawa H, Inazumi Y, Masaki T, Hirata T, Yamaguchi A. Indole induces the
785 expression of multidrug exporter genes in Escherichia coli. Mol Microbiol. 2005
786 Feb;55(4):1113–26.

787 59. Martino PD, Fursy R, Bret L, Sundararaju B, Phillips RS. Indole can act as an
788 extracellular signal to regulate biofilm formation of Escherichia coli and other indole-
789 producing bacteria. Can J Microbiol. 2003 Jul;49(7):443–9.

790 60. Chant EL, Summers DK. Indole signalling contributes to the stable maintenance of
791 Escherichia coli multicopy plasmids. Mol Microbiol. 2007;63(1):35–43.

792 61. Queen J, Domingue JC, White JR, Stevens C, Udayasuryan B, Nguyen TTD, et al.
793 Comparative Analysis of Colon Cancer-Derived Fusobacterium nucleatum
794 Subspecies: Inflammation and Colon Tumorigenesis in Murine Models. mBio. 2022
795 Feb 8;13(1):e02991-21.

796 62. Kostic AD, Chun E, Robertson L, Glickman JN, Gallini CA, Michaud M, et al.
797 Fusobacterium nucleatum potentiates intestinal tumorigenesis and modulates the
798 tumor immune microenvironment. Cell Host Microbe. 2013 Aug 14;14(2):207–15.

799 63. Cochrane K, Robinson AV, Holt RA, Allen-Vercoe E. A survey of Fusobacterium
800 nucleatum genes modulated by host cell infection. Microb Genomics. 2020
801 Feb;6(2):e000300.

802 64. Zhao T, Chen J, Liu S, Yang J, Wu J, Miao L, et al. Transcriptome analysis of
803 *Fusobacterium nucleatum* reveals differential gene expression patterns in the biofilm
804 versus planktonic cells. Biochem Biophys Res Commun. 2022 Feb 19;593:151–7.

805 65. Choudhury A, Scano C, Barton A, Greathouse KL. Targeted therapy of oncomicrobe
806 F. nucleatum with bioengineered probiotic expressing guided antimicrobial peptide
807 (gAMP) [Internet]. bioRxiv; 2024 [cited 2025 Apr 16]. p. 2024.10.29.620919.
808 Available from: https://www.biorxiv.org/content/10.1101/2024.10.29.620919v1

809 66. Pan S, Underhill SAM, Hamm CW, Stover MA, Butler DR, Shults CA, et al. Glycerol
810 metabolism impacts biofilm phenotypes and virulence in Pseudomonas aeruginosa
811 via the Entner-Doudoroff pathway. mSphere. 9(4):e00786-23.

67. Sinha AK, Laursen MF, Brinck JE, Rybtke ML, Hjørne AP, Procházková N, et al. Dietary fibre directs microbial tryptophan metabolism via metabolic interactions in the gut microbiota. Nat Microbiol. 2024 Aug;9(8):1964–78.

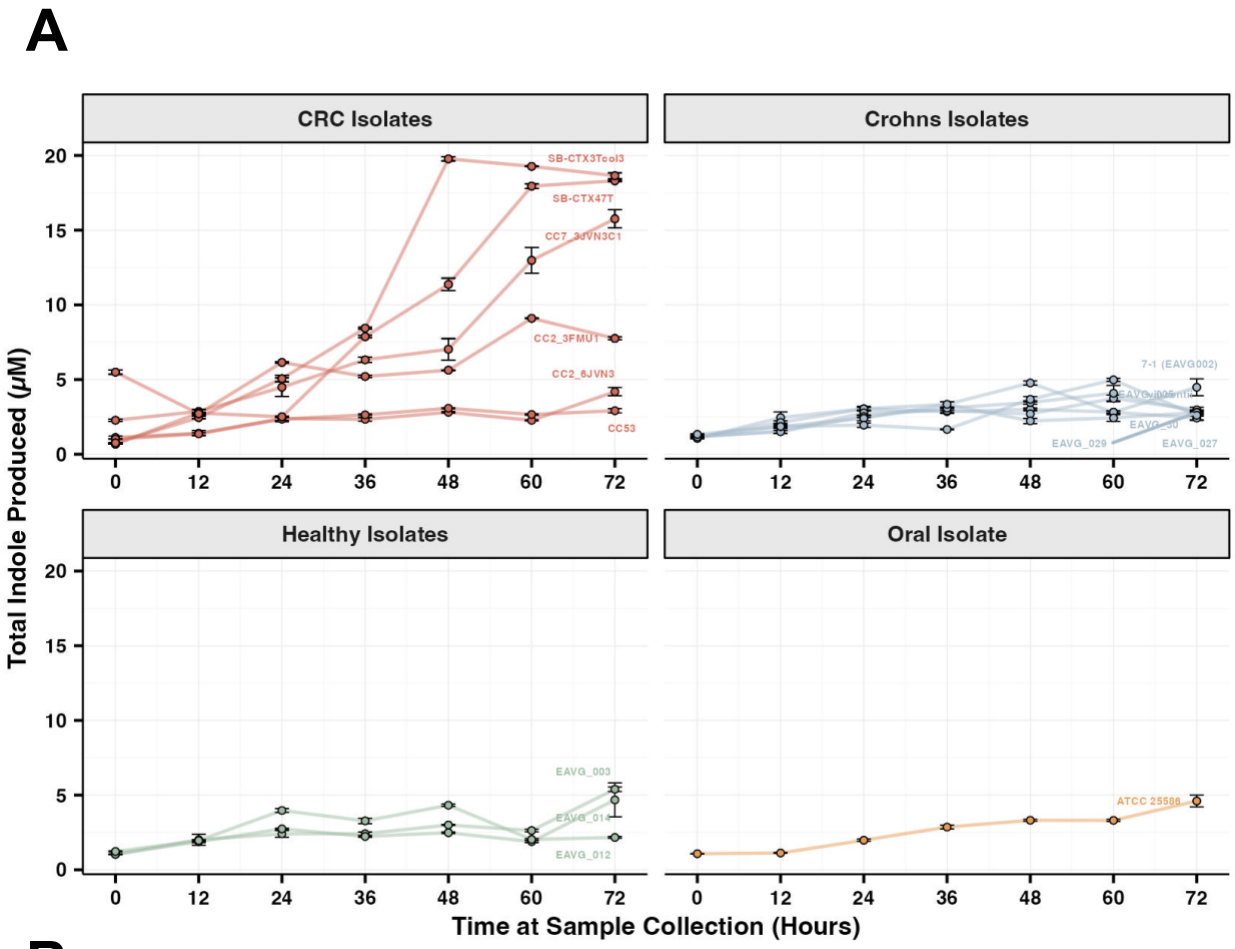
A
CRC Isolates
Crohns Isolates
Healthy Isolates
Oral Isolate
Total Indole Produced (μM)
Time at Sample Collection (Hours)
SB-CTX3Tool3
SB-CTX47T
CC7_3JVN3C1
CC2_3FMU1
CC2_6JVN3
CC53
7-1 (EAVG002)
EAVG_029
EAVG_027
EAVG_003
EAVG_012
ATCC 25586

826

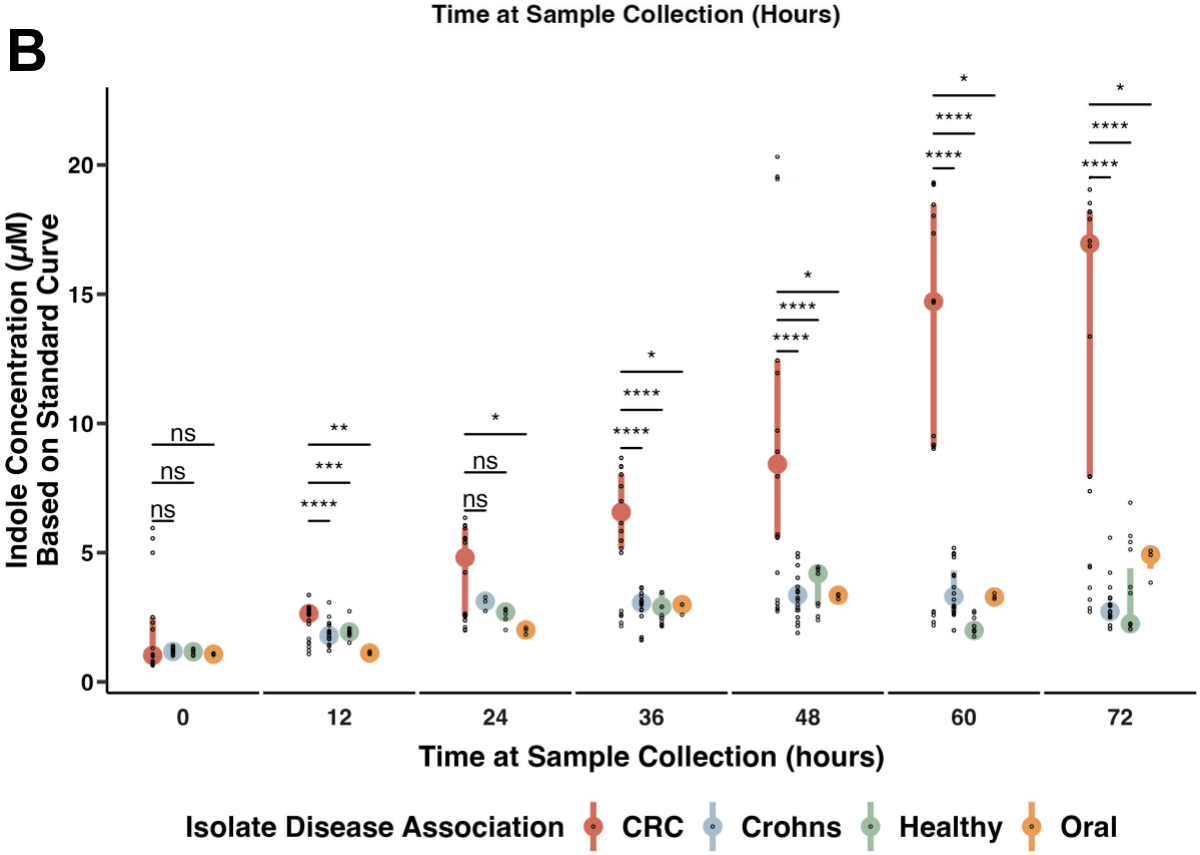
B
Indole Concentration (μM) Based on Standard Curve
Time at Sample Collection (hours)
Isolate Disease Association
CRC
Crohns
Healthy
Oral

827

Figure 1: Elevated indole production is a distinctive feature of colorectal cancer-associated *F. nucleatum* isolates. (1A) Total indole production by each *F. nucleatum* isolate over time quantified using Kovac's reagent and calibrated against a standard curve. The Kovacs reagent (p-dimethylaminobenzaldehyde in acidic solution) reacts with the indole ring at position 3, forming a conjugated imine that produces a characteristic pink/red color, with the intensity proportional to the total indole concentration. Data is presented as the mean total indole production (μM concentration), with error bars indicating the standard error of the mean (SEM) for the individual isolate. **(1B)** Total indole production of *F. nucleatum* isolates over time grouped by isolate disease association. An adjusted ANOVA was performed using the Benjamini-Hochberg method to compare total indole production between CRC-associated *F. nucleatum* isolates and non-CRC isolates. The Tukey's HSD test was then applied to identify significant pairwise differences. Data is represented as the median, with the interquartile range (IQR) capturing the central 50% of the data distribution. p values are indicated as follows: * $p < 0.05$; ** $p < 0.01$; *** $p < 0.001$; **** $p < 0.0001$. Isolates grouped by disease association (CRC: n=6, Crohn's: n=6, healthy: n=3, oral lesion: n=1).

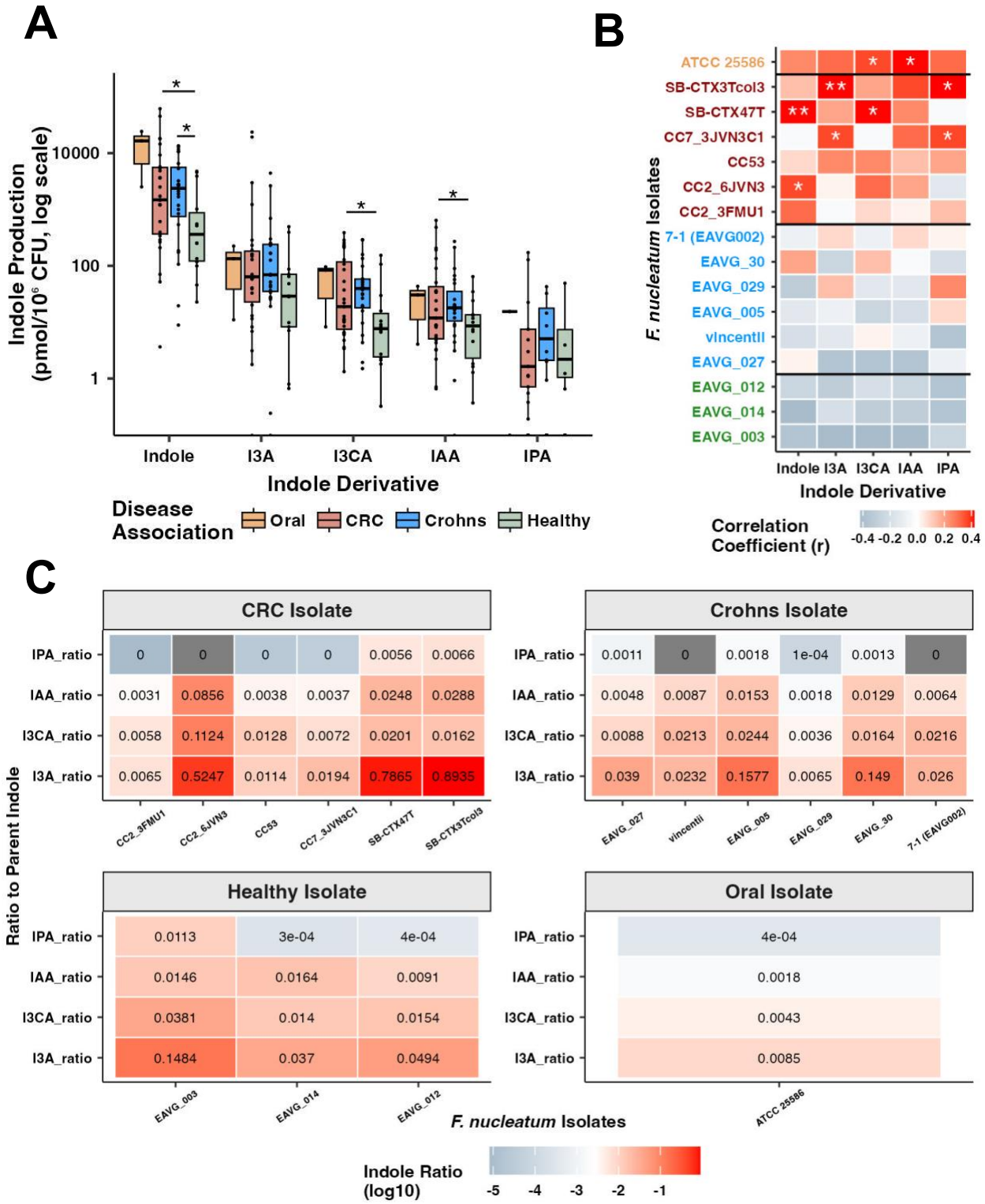
A
Indole Production (pmol/10^6 CFU, log scale)
10000
100
1
Indole
I3A
I3CA
IAA
IPA
Indole Derivative
Disease Association
Oral
CRC
Crohns
Healthy
B
F. nucleatum Isolates
ATCC 25586
SB-CTX3Tcol3
SB-CTX47T
CC7_3JVN3C1
CC53
CC2_6JVN3
CC2_3FMU1
7-1 (EAVG002)
EAVG_30
EAVG_029
EAVG_005
vincentii
EAVG_027
EAVG_012
EAVG_014
EAVG_003
Indole I3A I3CA IAA IPA
Indole Derivative
Correlation Coefficient (r)
-0.4 -0.2 0.0 0.2 0.4
C
Ratio to Parent Indole
CRC Isolate
IPA_ratio 0 0 0 0 0.0056 0.0066
IAA_ratio 0.0031 0.0856 0.0038 0.0037 0.0248 0.0288
I3CA_ratio 0.0058 0.1124 0.0128 0.0072 0.0201 0.0162
I3A_ratio 0.0065 0.5247 0.0114 0.0194 0.7865 0.8935
CC2_3FMU1 CC2_6JVN3 CC53 CC7_3JVN3C1 SB-CTX47T SB-CTX3Tcol3
Crohns Isolate
IPA_ratio 0.0011 0 0.0018 1e-04 0.0013 0
IAA_ratio 0.0048 0.0087 0.0153 0.0018 0.0129 0.0064
I3CA_ratio 0.0088 0.0213 0.0244 0.0036 0.0164 0.0216
I3A_ratio 0.039 0.0232 0.1577 0.0065 0.149 0.026
EAVG_027 vincentii EAVG_005 EAVG_029 EAVG_30 7-1 (EAVG002)
Healthy Isolate
IPA_ratio 0.0113 3e-04 4e-04
IAA_ratio 0.0146 0.0164 0.0091
I3CA_ratio 0.0381 0.014 0.0154
I3A_ratio 0.1484 0.037 0.0494
EAVG_003 EAVG_014 EAVG_012
Oral Isolate
IPA_ratio 4e-04
IAA_ratio 0.0018
I3CA_ratio 0.0043
I3A_ratio 0.0085
ATCC 25586
F. nucleatum Isolates
Indole Ratio (log10)
-5 -4 -3 -2 -1

Figure 2: Disease-associated isolates exhibit elevated production of specific indole derivatives and have distinct indole production profiles. (2A) Quantification of indole and indole derivatives in Columbia Broth spent media from *F. nucleatum* clinical isolates by HPLC. Box plots illustrate the production of five indole compounds - indole, indole-3-aldehyde (I3A), indole-3-carboxylic acid (I3CA), indole-3-acetic acid (IAA), and indole-3-propionic acid (IPA) - measured in picomoles (pmol) per million colony-forming units (CFU). P-values indicate statistically significant differences between groups, determined by one-way ANOVA. **(2B)** *F. nucleatum* isolates were transformed into binary valures, and a Point-Biserial correlation analysis was performed. The resulting heatmap depicts Pearson correlation coefficients (ρ) between *F. nucleatum* isolates and the production levels of specific indole derivatives. The y-axis labels are color-coded based on the disease association of each isolate: green for healthy, blue for Crohn's disease, red for CRC, and orange for oral isolate. Positive correlations are indicated in shades of red, while negative correlations are shown in shades of blue. Asterisks (*) denote statistically significant correlations (* $p < 0.05$; ** $p < 0.01$). **(C)** To determine indole derivative production preference by isolates, ratios of indole derivatives to the parent indole were generated for all *F. nucleatum* isolates. Each cell shows the ratio value, with colors ranging from light blue (low ratios) to red (high ratios). Isolates grouped by disease association (CRC: n=6, Crohn's: n=6, healthy: n=3, oral lesion: n=1).

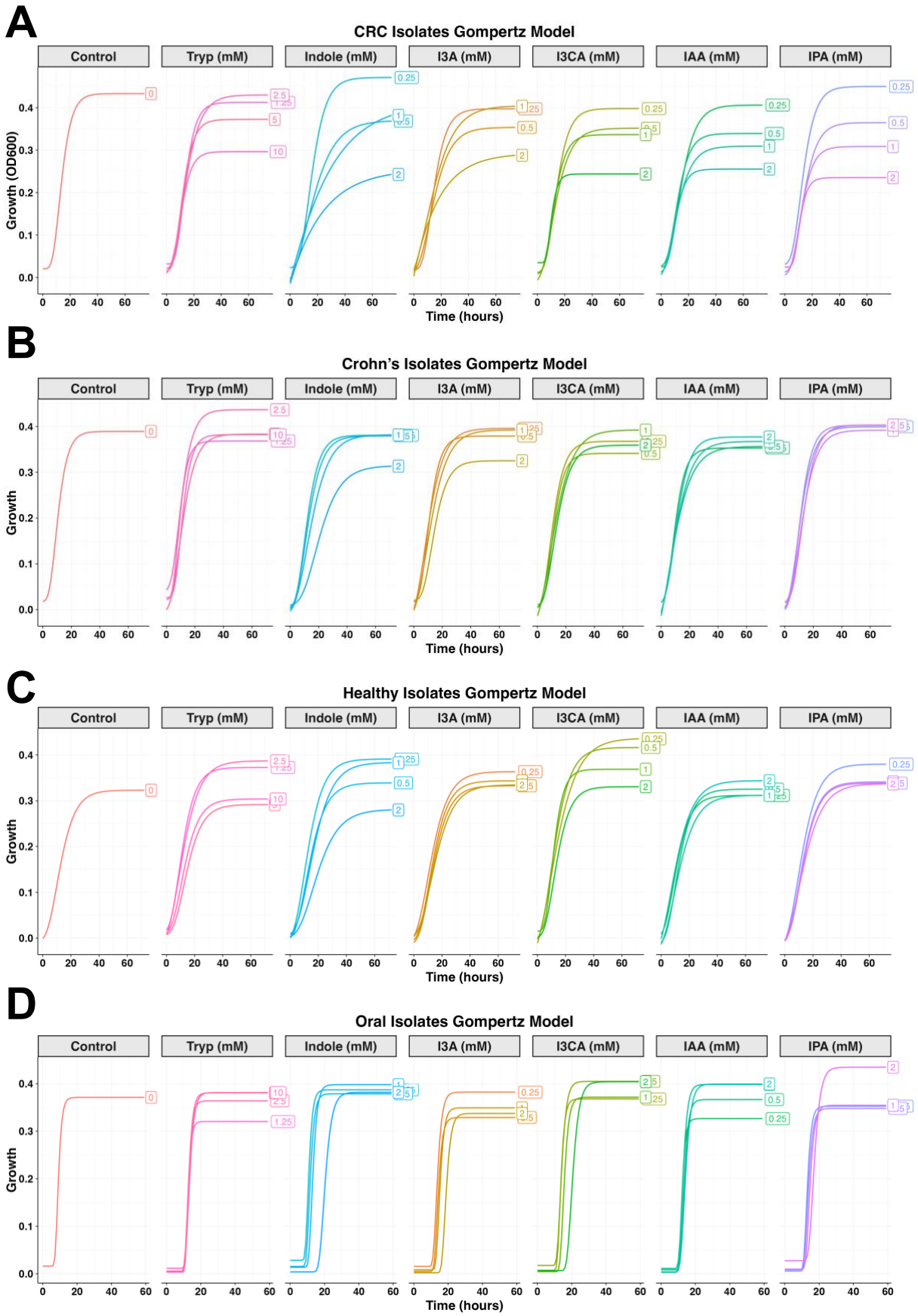
A
CRC Isolates Gompertz Model
Control
Tryp (mM)
Indole (mM)
I3A (mM)
I3CA (mM)
IAA (mM)
IPA (mM)
Growth (OD600)
Time (hours)
B
Crohn's Isolates Gompertz Model
Growth
Time (hours)
C
Healthy Isolates Gompertz Model
Growth
Time (hours)
D
Oral Isolates Gompertz Model
Growth
Time (hours)

Figure 3 Exposure to indole derivatives alter *F. nucleatum* growth kinetics in a dose-dependent manner without bactericidal effects. Gompertz growth models comparing bacterial growth responses to indole derivatives across CRC **(3A)**, Crohn's **(3B)**, Healthy **(3C)**, and Oral isolates **(3D)**. Growth (OD) versus time curves show responses to Indole, I3A, I3CA, IAA, and IPA (all in mM). Chloramphenicol (µg/mL) are used as negative controls to display strong inhibition of growth (**Supplemental Figure 3**). Tryptophan was included in these growth experiments to determine whether the bacteria's ability to convert tryptophan to indole compounds impacts their growth. Growth was monitored for 72 hours, with concentrations of treatments indicated on each curve. Gompertz model fits generated key growth parameters including inflection time, growth rate, upper asymptote (OD max), initial value, R-squared, and maximum growth rate to quantitatively compare derivatives effects across isolates (Table 3-6). Isolates grouped by disease association (CRC: n=6, Crohn's: n=6, healthy: n=3, oral lesion: n=1).

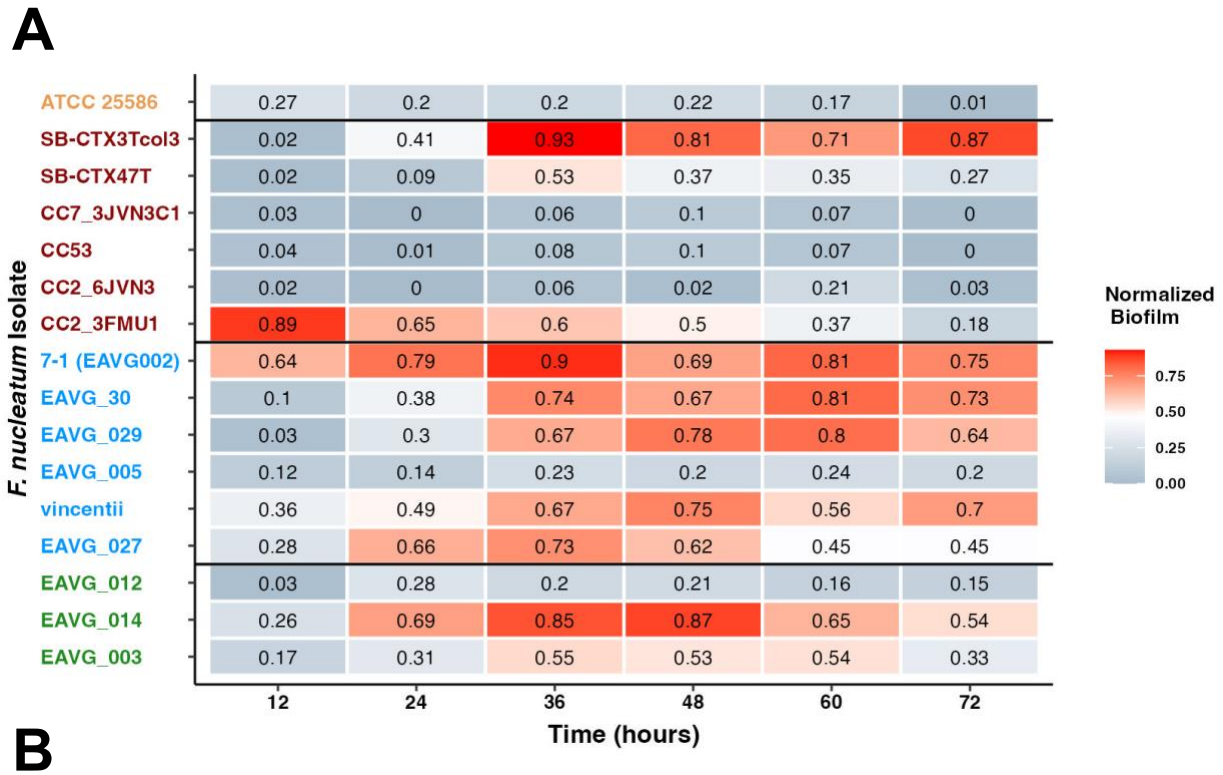

919

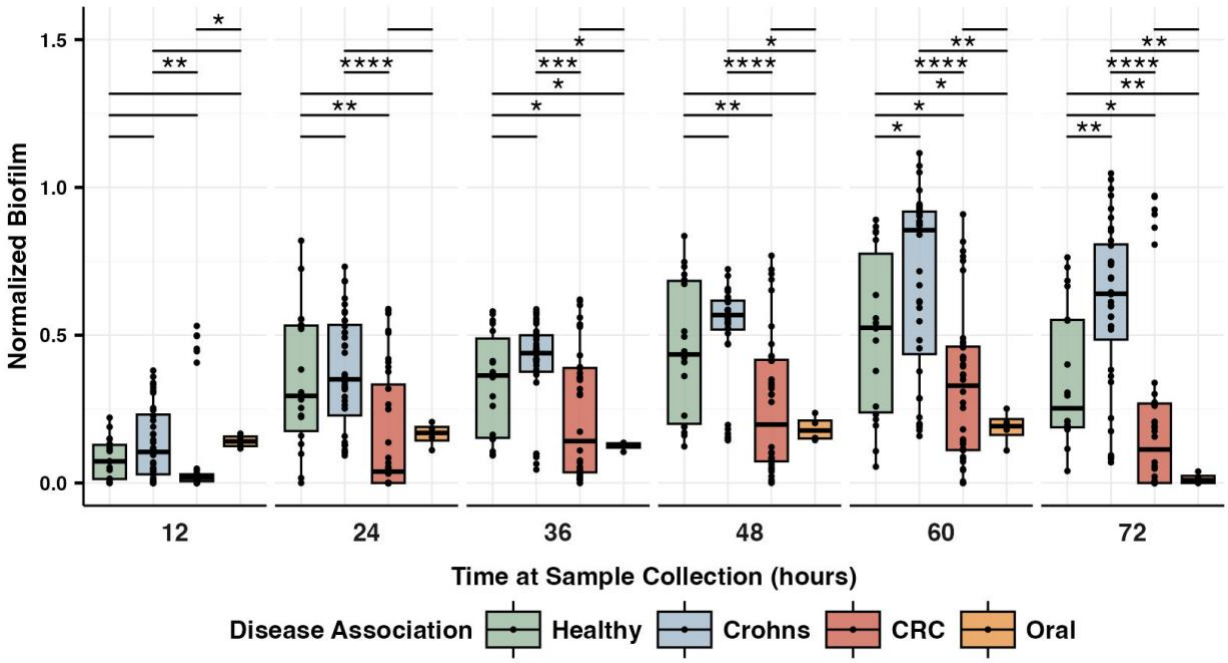

920
921
922

923

924

Figure 4: Biofilm Formation Profiles Distinguish Disease-Associated *F. nucleatum* Isolates. We evaluated the temporal biofilm formation patterns of bacterial isolates to identify high biofilm-producing isolates. **(4A)** Biofilm formation was quantified at six time points (12, 24, 36, 48, 60, and 72 hours) across four study groups (Healthy, Crohn's, CRC, and Oral), with measurements normalized to the maximum biofilm value at each time point. An adjusted ANOVA was performed using the Benjamini-Hochberg method to compare total indole production between grouped *F. nucleatum* isolate. The Tukey's HSD test was then applied to identify significant pairwise differences. Asterisks indicate statistical significance (* $p<0.05$, ** $p<0.01$, *** $p<0.001$, **** $p<0.0001$). **(4B)** Heatmap visualizing temporal biofilm formation patterns across Fusobacterium isolates (Fuso1-25), with normalized values represented by a white-to-red color gradient. The intensity of red coloration corresponds to biofilm strength, and numerical values indicate the proportion of maximum biofilm formation observed at that time point. Isolates grouped by disease association (CRC: n=6, Crohn's: n=6, healthy: n=3, oral lesion: n=1).

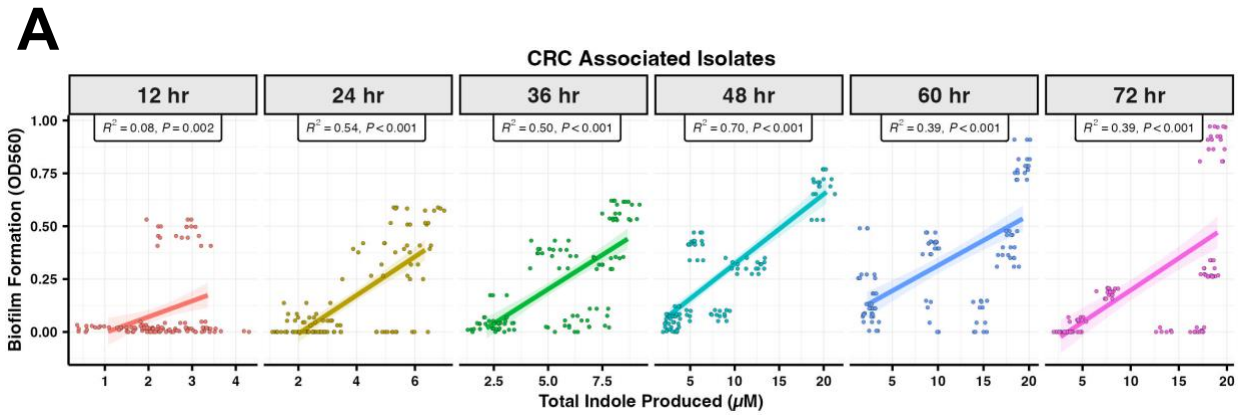

967
968

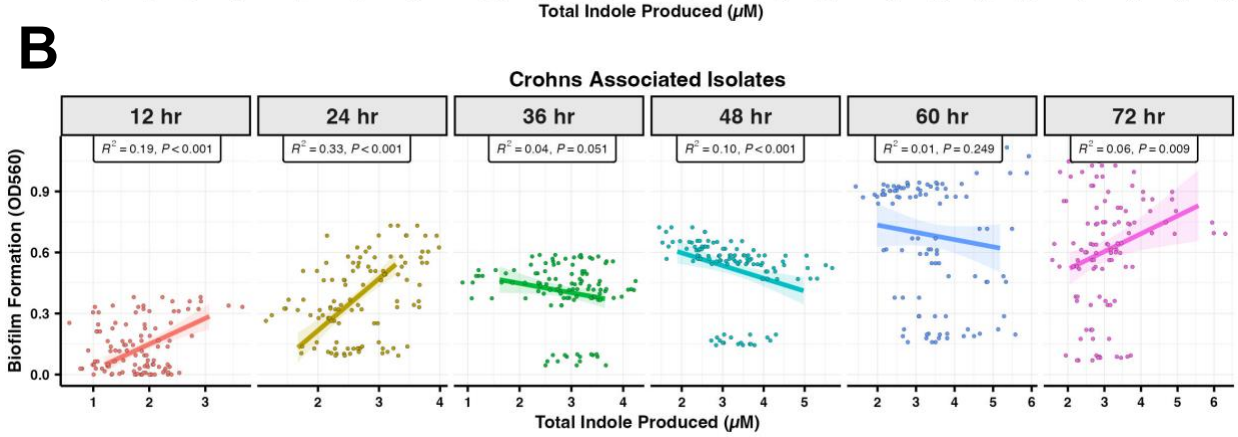

969
970

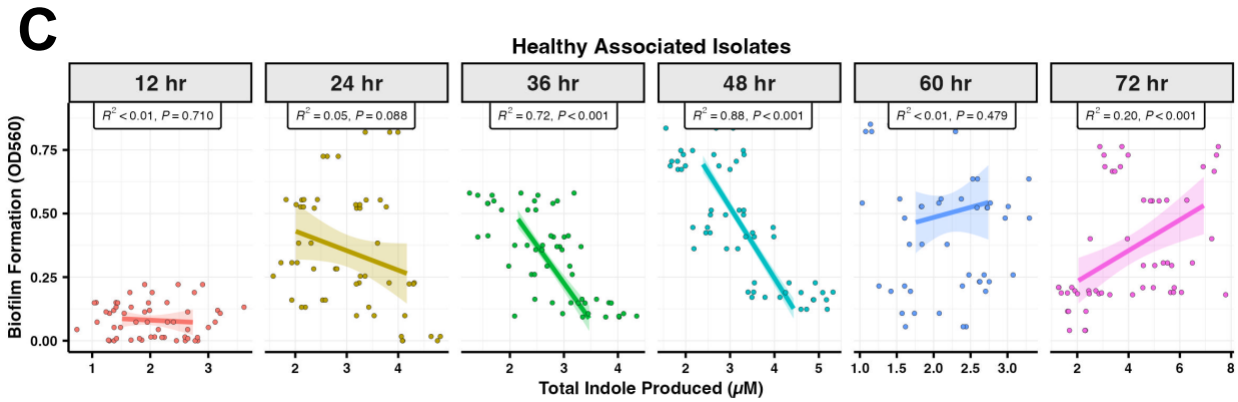

971
972

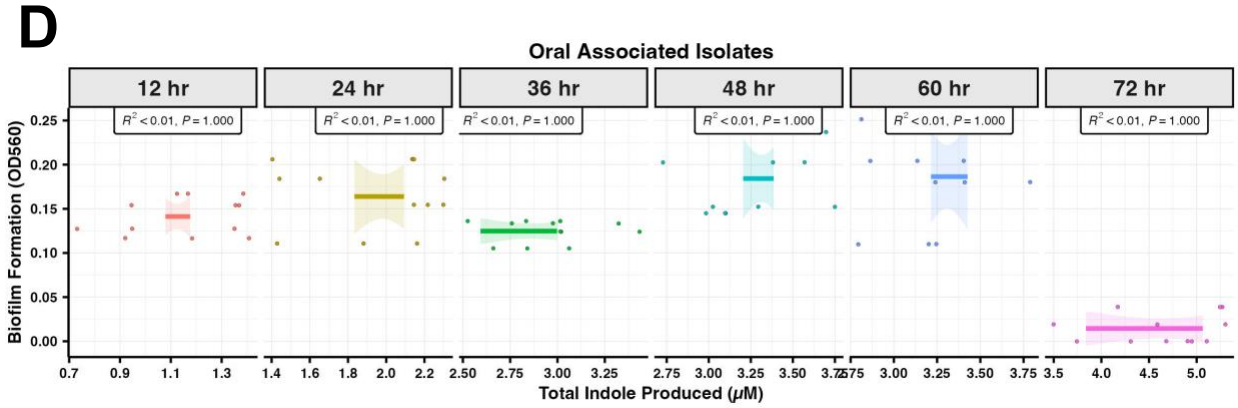

973
974

975 **Figure 5: Biofilm formation by CRC-associated *F. nucleatum* isolates is positively**
976 **correlated with total indole production.** The relationship between total indole
977 production (μM) and biofilm formation (OD_{590}) was analyzed over time in bacterial isolates
978 from different sources: **(5A)** CRC, **(5B)** Crohn's, **(5C)** healthy, and **(5D)** oral-associated
979 isolates. Measurements were collected at 12, 24, 36, 48, 60, and 72 hours. Each point
980 represents data from a single bacterial isolate, with biofilm formation and total indole
981 production determined through independent parallel experiments conducted under
982 identical growth conditions. Pearson correlation analysis was performed, and regression
983 lines with 95% confidence intervals (shaded areas) are shown for each time point.
984 Isolates grouped by disease association (CRC: n=6, Crohn's: n=6, healthy: n=3, oral
985 lesion: n=1).

986
987
988
989
990
991
992
993
994
995
996
997
998

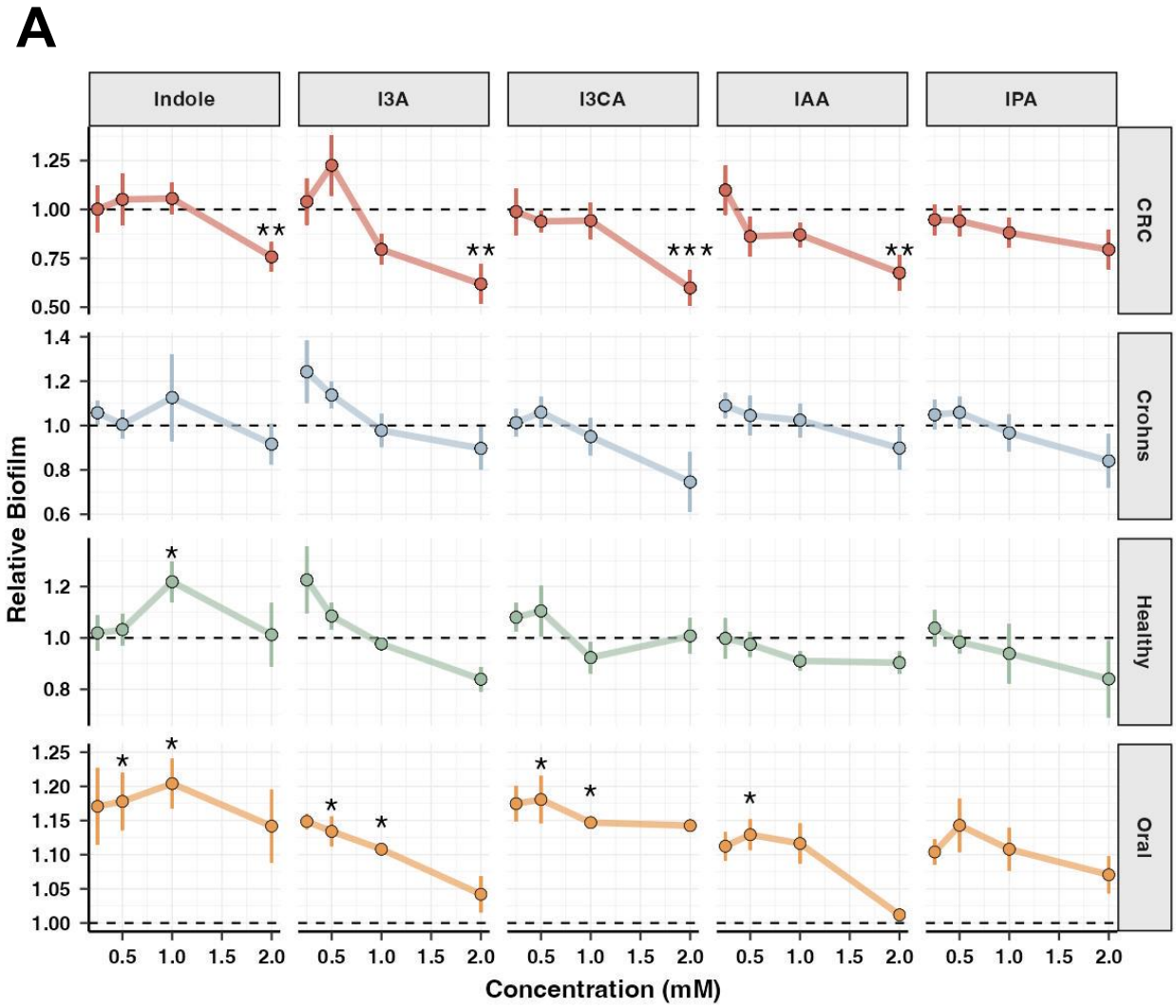

Figure 6: Exposure to Indole Derivatives Significantly Diminish Biofilm Formation in CRC-Associated *F. nucleatum* Isolates: Indole-induced changes in biofilm formation were assessed at concentrations ranging from 0.5 to 2.0 mM. Baseline biofilm formation is indicated by dotted lines, and relative changes from baseline biofilm (relative) across treatment concentration was quantified. Statistical comparisons between treated and control samples were performed using adjusted ANOVA with Benjamini-Hochberg correction, followed by Tukey's HSD test for pairwise comparisons. Statistical significance levels are denoted by asterisks (* $p<0.05$, ** $p<0.01$, *** $p<0.001$, **** $p<0.0001$). Isolates grouped by disease association (CRC: n=6, Crohn's: n=6, healthy: n=3, oral lesion: n=1).

A

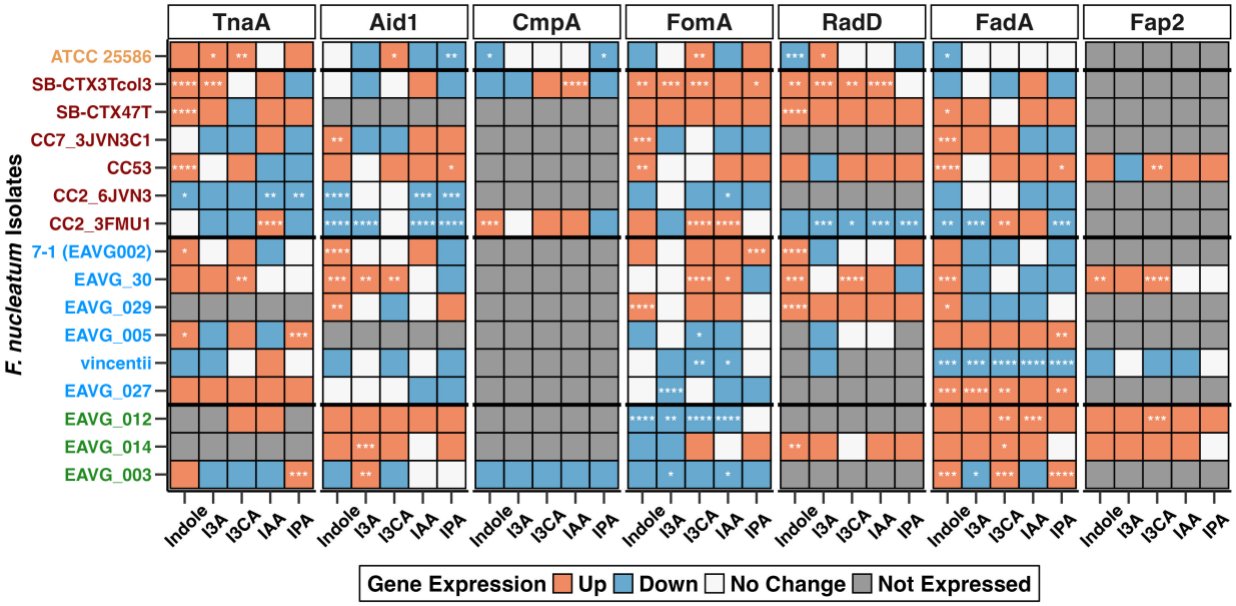

B

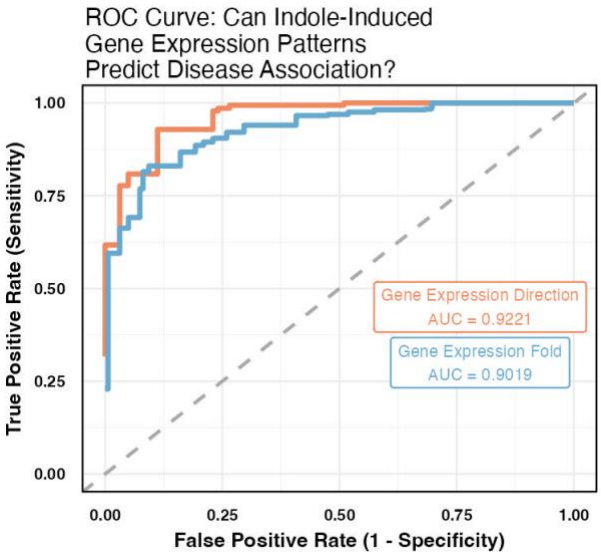

Gene Expression Direction: Confusion Matrix and Statistics			
	CRC	Crohn's	Healthy
CRC	119	32	19
Crohn's	37	127	1
Healthy	6	2	61
Accuracy:	0.7599		
P-Value:	< 2e-16		

Gene Expression Fold: Confusion Matrix and Statistics			
	CRC	Crohn's	Healthy
CRC	118	1	26
Crohn's	44	149	24
Healthy	0	11	31
Accuracy:	0.7376		
P-Value:	< 2.2e-16		

Figure 7: Indole Derivatives Elicit Distinct Virulence Expression Patterns in *F. nucleatum* Based on Isolate Origin and Disease-Association. (7A) Heatmap shows expression changes in virulence genes after exposure to indole derivatives for each isoalte. Each cell indicates the direction of gene expression in response to treatment relative to untreated controls. Threshold is as follows: fold>1.25 = "Up", 1.25>fold>0.75 = “No change”, fold<0.75 = “Down”. Color coding: red = upregulation, blue = downregulation, white = no significant change, gray = gene not expressed. Pairwise t-tests (vs. DMSO) were performed within each isolate and target group. Bonferroni correction was applied for multiple comparisons. Asterisks represent statistical significance: (* $p<0.05$, ** $p<0.01$, *** $p<0.001$, **** $p<0.0001$). **(7B)** A naïve Bayes classification model was used to determine whether there exists a specific indole response by each disease state. Due to having only 1 isolate, the oral lesion was excluded from the classifer. The gene expression fold data and the gene expression direction calculated with the threshold mentioned above was split into training (70%) and test data (30%). Disease states were classified using a Naive Bayes model with kernel density estimation implemented in R. The Naive Bayes classifier was trained using the formula disease ~., indicating that all available features were utilized as predictors of disease status. Isolates grouped by disease association (CRC: n=6, Crohn's: n=6, healthy: n=3).

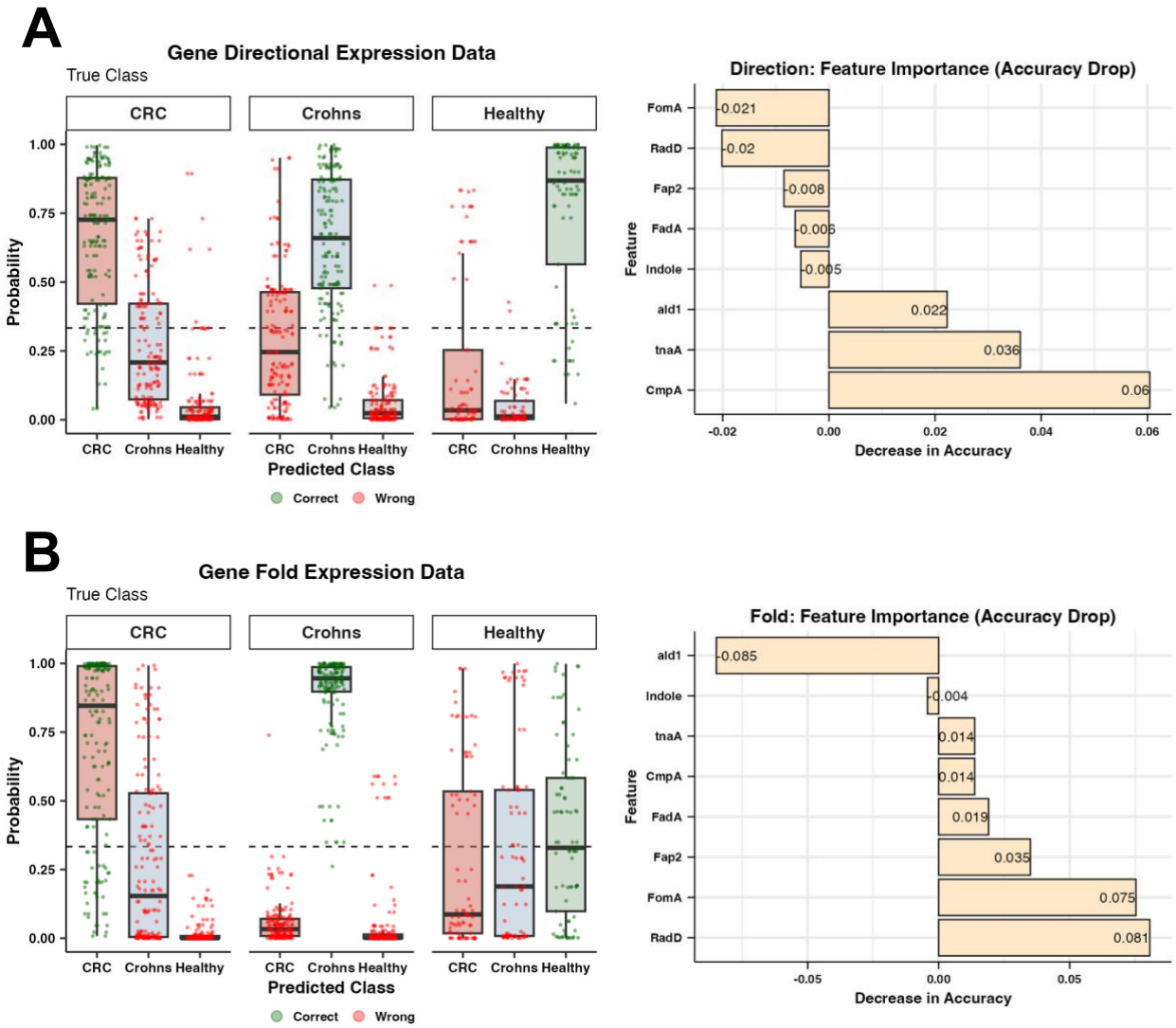

Figure 8: Naive Bayes posterior probabilities and feature importance reveal class-specific predictive confidence based on gene expression direction and fold change. Posterior class probabilities from a Naive Bayes classifier trained on gene expression direction (left) or fold change values (right) across three disease states: CRC, Crohn's disease, and healthy controls **(8A)**. Each boxplot represents the predicted probability distribution for each class, stratified by the true class (facet labels). Dots represent individual predictions, colored by classification accuracy (green = correct, red = wrong). The dashed horizontal line indicates the probability of random classification (1/3). Feature importance plots showing the decrease in model accuracy when each gene was removed **(8B)**. Left: Direction-based model. Right: Fold change-based model. Bars represent the mean change in classification accuracy across cross-validation folds. Isolates grouped by disease association (CRC: n=6, Crohn's: n=6, healthy: n=3).

Table 1: Sources and References of Clinical *F. nucleatum* Isolates

STRAIN	ORIGIN	DISEASE	SUBSPECIES	ISOLATE SUPPLIERS
F. nucleatum animalis EAVG_003	Nonspecific colon biopsy	**Healthy**	*animalis*	Dr. Emma Allen-Vercoe, University of Guelph
F. nucleatum EAVG_014	Rectum biopsy	**Healthy**	*vincentii*	Dr. Emma Allen-Vercoe, University of Guelph
F. nucleatum EAVG_012	Ascending colon biopsy	**Healthy**	*vincentii*	Dr. Emma Allen-Vercoe, University of Guelph
F. nucleatum EAVG_027	Distal colon biopsy	**Crohn's (remission)**	*animalis*	Dr. Emma Allen-Vercoe, University of Guelph
F. nucleatum subsp. vincentii	Distal colon biopsy	**Crohn's (remission)**	*vincentii*	Dr. Emma Allen-Vercoe, University of Guelph
F. nucleatum EAVG_005	Sigmoid colon biopsy	**Crohn's (remission)**	*nucleatum*	Dr. Emma Allen-Vercoe, University of Guelph
F. nucleatum EAVG_029	Ascending colon biopsy	**Crohn's (active)**	*vincentii*	Dr. Emma Allen-Vercoe, University of Guelph
F. nucleatum EAVG_030	Ascending colon biopsy	**Crohn's (active)**	*vincentii*	Dr. Emma Allen-Vercoe, University of Guelph
F. nucleatum subsp. nucleatum CC2_3FMU1	Tumor biopsy	**Colorectal cancer**	*nucleatum*	Dr. Emma Allen-Vercoe, University of Guelph
F. nucleatum subsp. animalis CC2_6JVN3	Tumor biopsy	**Colorectal cancer**	*animalis*	Dr. Emma Allen-Vercoe, University of Guelph
F. nucleatum subsp. vincentii CC53	Tumor biopsy	**Colorectal cancer**	*vincentii*	Dr. Emma Allen-Vercoe, University of Guelph
F. nucleatum subsp. animalis CC7_3JVN3C1	Tumor biopsy	**Colorectal cancer**	*animalis*	Dr. Emma Allen-Vercoe, University of Guelph
F. nucleatum (SB-CTX47T)	Tumor biopsy	**Colorectal cancer**	*polymorphum*	Dr. Susan Bullman, MD Anderson Cancer Center
F. nucleatum (SB-CTX3Tcol3)	Tumor biopsy	**Colorectal cancer**	*nucleatum*	Dr. Susan Bullman, MD Anderson Cancer Center
F. nucleatum EAVG002-7_1-HM_73	Ascending colon biopsy	**Crohn's (active)**	*animalis*	Dr. Emma Allen-Vercoe, University of Guelph
F. nucleatum subsp. nucleatum Knorr 25586	ATCC	**Oral Lesion**	*nucleatum*	ATCC

1094
1095
1096
1097
1098
1099
1100
1101
1102
1103
1104
1105
1106
1107

Table 2: *F. nucleatum* Virulence Factor and Subspecies Primers

PRIMER	SEQUENCE	TARGET	REFERENCES
FadA FWD	GCTAGACAAGCACTAGCACAA	Fusobacterium adhesin A (FadA)	In house
FadA REV	CTTGTGTTAAGCTTCTGCTTGAAGT		
Fap2 FWD	GGAACAAGGAAATCAAGTGGTAAA	Fap2	
Fap2 REV	GCTTTGTCTCCTCTTTTATATTC		
tnaA FWD	CGTGCATTAAAAGCAACTCACTATAATG	Tryptophanase enzyme	
tnaA REV	CAGTAGTTCCCGAGTCTGATAAC		
aid1 FWD	TACAGGAGGTGCCGTAGCAG	aid1 (Adherence Inducing Determinant 1)	[4]
aid1 REV	TTTTTGTTAATTCTCCAGCTCCA		
16s FWD	TTGGACAATGGACCGAGAGT	16S rRNA	
16s REV	GCCGTCACTTCTTCTGTTGG		
CmpA FWD	TTGGGATCAAGGAAAACATCAATTAGG	coaggregation mediating protein A (CmpA)	[30]
CmpA REV	ATAATTCCTTTATTATCTCCCATATAAGCAATACC		
RadD FWD	GGATTTATCTTTGCTAATTGGGGAAATTATAG	Fn1526 (now designated as radD)	
RadD REV	ACTATTCCATATTCTCCATAATATTTCCCATTAGA		
FomA FWD	AGAGTTTGATCCTGGCTCAG	outer membrane protein porin (FomA)	
FomA REV	GTCATCGTGCACACAGAATTGCTG		
Subsp. animalis FWD	TTTGTATTTGACAATTTAATTAGAGCA	Subspecies-specific PCR: Fn. animalis hypothetical protein gene CDS, Forwardprimer	[31]
Subsp. animalis REV	TGGGATAATAATCCAAATATYGCAC		
Subsp. nucleatum FWD	CTTCATTGTTAGGATTACAAGAATAGGC	Subspecies-specific PCR: Fn. nucleatum Ankyrin repeat protein gene CDS, Reverse primer:	
Subsp. nucleatum REV	TTTCAGTAACATTTATTGGGAGGTTT		
Subsp. polymorphum FWD	AAGATTAAATAAAGATGGAAATAACCATRAA	Subspecies-specific PCR: Fn. polymorphum hypothetical protein gene CDS, Reverse primer:	
Subsp. polymorphum REV	CCATCTCCAAAGCCTTTCC		
Subsp. vincentii FWD	CTTTGTCTTATGATTTATTGCRTATCTTC	Subspecies-specific PCR: Fn. vincentii hypothetical protein gene CDS, Reverse primer:	
Subsp. vincentii REV	GAAGAATCAGAAGCACTACCAGCA		

Table 3: CRC Gompertz Model Parameters							
	Concentration	Inflection Time	Growth Rate	OD MAX	Initial Value	R squared	Max Growth Rate
Control	0	11.96	0.20	0.43	0.02	0.35	0.03
Tryp (mM)	1.25	11.86	0.20	0.41	0.03	0.32	0.03
	2.5	11.03	0.13	0.43	0.00	0.39	0.02
	5	10.04	0.19	0.37	0.02	0.27	0.02
	10	9.35	0.21	0.30	0.02	0.23	0.02
Indole (mM)	0.25	13.62	0.15	0.47	0.02	0.40	0.02
	0.5	11.84	0.09	0.37	-0.03	0.28	0.01
	1	-21.20	0.04	0.41	-0.78	0.23	0.02
	2	-74.89	0.04	0.26	-6.13	0.14	0.10
I3A (mM)	0.25	12.49	0.16	0.40	0.02	0.30	0.02
	0.5	11.49	0.12	0.35	0.01	0.23	0.02
	1	9.46	0.09	0.40	-0.02	0.25	0.01
	2	-92.97	0.05	0.29	-47.33	0.14	0.96
I3CA (mM)	0.25	11.74	0.17	0.40	0.01	0.29	0.02
	0.5	10.28	0.13	0.35	-0.01	0.25	0.02
	1	10.29	0.18	0.34	0.01	0.28	0.02
	2	9.16	0.34	0.24	0.03	0.12	0.03
IAA (mM)	0.25	11.73	0.14	0.41	0.01	0.32	0.02
	0.5	10.13	0.17	0.34	0.03	0.24	0.02
	1	9.02	0.14	0.31	0.00	0.22	0.02
	2	9.37	0.22	0.26	0.02	0.15	0.02
IPA (mM)	0.25	11.18	0.16	0.40	0.03	0.26	0.02
	0.5	11.24	0.15	0.36	0.00	0.25	0.02
	1	10.45	0.18	0.31	0.01	0.18	0.02
	2	9.80	0.28	0.24	0.02	0.14	0.02

Table 4: Crohn's Gompertz Model Parameters							
	Concentration	Inflection Time	Growth Rate	OD MAX	Initial Value	R squared	Max Growth Rate
Control	0	8.96	0.22	0.39	0.02	0.33	0.03
Tryp (mM)	1.25	7.92	0.27	0.37	0.02	0.28	0.03
	2.5	8.55	0.19	0.44	0.04	0.31	0.03
	5	9.06	0.16	0.38	-0.01	0.37	0.02
	10	9.80	0.23	0.38	0.03	0.33	0.03
Indole (mM)	0.25	9.82	0.17	0.38	0.00	0.34	0.02
	0.5	10.29	0.15	0.38	0.00	0.37	0.02
	1	11.72	0.12	0.38	-0.01	0.42	0.02
	2	17.44	0.10	0.31	0.01	0.47	0.01
I3A (mM)	0.25	7.67	0.14	0.40	-0.02	0.31	0.02
	0.5	9.10	0.20	0.38	0.02	0.29	0.03
	1	8.91	0.12	0.39	-0.02	0.36	0.02
	2	12.28	0.16	0.33	0.02	0.41	0.02
I3CA (mM)	0.25	8.74	0.18	0.37	0.00	0.31	0.02
	0.5	9.65	0.21	0.34	0.01	0.29	0.03
	1	8.78	0.12	0.39	-0.04	0.35	0.02
	2	11.03	0.15	0.36	0.00	0.37	0.02
IAA (mM)	0.25	8.22	0.21	0.35	0.01	0.31	0.03
	0.5	5.53	0.11	0.36	-0.08	0.30	0.02
	1	7.56	0.13	0.37	-0.03	0.30	0.02
	2	9.17	0.17	0.38	0.01	0.42	0.02
IPA (mM)	0.25	8.79	0.16	0.40	0.00	0.35	0.02
	0.5	9.30	0.19	0.40	0.01	0.36	0.03
	1	9.78	0.15	0.39	-0.01	0.34	0.02
	2	11.07	0.16	0.40	0.02	0.41	0.02

Table 5: Healthy Gompertz Model Parameters							
	Concentration	Inflection Time	Growth Rate	OD MAX	Initial Value	R squared	Max Growth Rate
Control	0	9.90	0.14	0.32	-0.01	0.26	0.02
Tryp (mM)	1.25	8.90	0.16	0.37	0.01	0.26	0.02
	2.5	8.84	0.12	0.39	-0.01	0.34	0.02
	5	12.09	0.14	0.29	0.01	0.26	0.01
	10	10.39	0.14	0.30	0.01	0.20	0.02
Indole (mM)	0.25	10.02	0.13	0.39	-0.01	0.24	0.02
	0.5	11.24	0.13	0.34	0.00	0.28	0.02
	1	13.43	0.11	0.38	0.00	0.42	0.02
	2	15.77	0.10	0.28	0.00	0.25	0.01
I3A (mM)	0.25	9.72	0.12	0.36	-0.01	0.29	0.02
	0.5	11.28	0.13	0.33	-0.01	0.32	0.02
	1	10.89	0.14	0.34	-0.01	0.30	0.02
	2	11.99	0.11	0.33	0.00	0.35	0.01
I3CA (mM)	0.25	9.13	0.10	0.44	-0.06	0.38	0.02
	0.5	9.60	0.13	0.42	-0.01	0.32	0.02
	1	9.96	0.22	0.37	0.02	0.27	0.03
	2	11.35	0.15	0.33	0.00	0.31	0.02
IAA (mM)	0.25	8.69	0.15	0.31	0.00	0.20	0.02
	0.5	10.04	0.15	0.33	-0.01	0.31	0.02
	1	9.27	0.12	0.31	-0.03	0.31	0.01
	2	6.84	0.12	0.34	-0.04	0.22	0.02
IPA (mM)	0.25	9.17	0.13	0.38	-0.02	0.25	0.02
	0.5	10.60	0.14	0.34	-0.01	0.22	0.02
	1	10.04	0.13	0.34	-0.01	0.23	0.02
	2	9.91	0.11	0.34	-0.03	0.25	0.01

Table 6: Oral Gompertz Model Parameters							
	Concentration	Inflection Time	Growth Rate	OD MAX	Initial Value	R squared	Max Growth Rate
Control	0	8.54	0.73	0.37	0.02	0.63	0.10
Tryp (mM)	1.25	12.19	0.84	0.32	0.00	0.48	0.10
	2.5	12.27	0.68	0.36	0.01	0.59	0.09
	5	12.27	0.62	0.38	0.00	0.66	0.09
	10	12.80	0.56	0.38	0.01	0.76	0.08
Indole (mM)	0.25	10.30	0.68	0.39	0.03	0.62	0.09
	0.5	11.08	0.61	0.38	0.02	0.66	0.08
	1	12.57	0.58	0.40	0.01	0.75	0.08
	2	19.46	0.38	0.38	0.00	0.88	0.05
I3A (mM)	0.25	13.07	0.55	0.38	0.02	0.70	0.07
	0.5	13.61	0.60	0.33	0.00	0.64	0.07
	1	14.61	0.61	0.35	0.01	0.75	0.08
	2	18.15	0.53	0.34	0.00	0.89	0.06
I3CA (mM)	0.25	13.09	0.67	0.37	0.01	0.66	0.09
	0.5	13.33	0.52	0.40	0.02	0.76	0.07
	1	14.95	0.56	0.37	0.00	0.78	0.08
	2	19.67	0.40	0.40	0.01	0.90	0.06
IAA (mM)	0.25	11.69	0.75	0.33	0.00	0.54	0.09
	0.5	12.73	0.59	0.37	0.01	0.65	0.08
	1	12.12	0.57	0.40	0.01	0.71	0.08
	2	13.40	0.46	0.40	0.00	0.77	0.07
IPA (mM)	0.25	12.59	0.65	0.35	0.01	0.67	0.08
	0.5	13.11	0.57	0.35	0.01	0.71	0.07
	1	14.03	0.56	0.35	0.01	0.75	0.07
	2	16.30	0.41	0.43	0.03	0.79	0.06